REPUBLIQUE ALGERIENNE DEMOCRATIQUE ET POPULAIRE
MINISTERE DE L'ENSEIGNEMENT SUPERIEURE ET DE LA RECHERCHE SCIENTIFIQUE

UNIVERSITE ABOU-BEKR BELKAID - TLEMCEN

MEMOIRE

Présenté à :

FACULTE DES SCIENCES – DEPARTEMENT DE PHYSIQUE

MASTER EN PHYSIQUE

Spécialité : Physique des Plasmas

Par :

Melle MEZOUAGH FARAH

Sur le thème

Laser-Induced Nanobubble Nucleation Around Plasmonic Nanoparticles.

Soutenu publiquement le 15 juin 2026 à Tlemcen devant le jury composé de :

LALLAM Farah	Maître de Conférences (B)	Université de Tlemcen	Présidente
SENOUDI Assia Rachida	Maître de Conférences (A)	Université de Tlemcen	Encadrante
BOUFATAH Mohammed Reda	Maître de Conférences (A)	Université de Tlemcen	Examinateur

MEZOUAGH/2026

Acknowledgements

First and foremost, I would like to express my sincere gratitude to Allah for granting me the strength and good health to complete this work.

I would like to express my deepest appreciation to my supervisor, **Dr. Senoudi Assia Rachida**, Associate Professor in the Department of Physics at the university Abu Bekr Belkaid Tlemcen for their valuable guidance, continuous support, constructive suggestions, and encouragement throughout the realization of this dissertation. Their expertise and advice have greatly contributed to the success of this work.

I am deeply honored and grateful to **Dr. Lallam Farah**, President of the Jury, Associate Professor in the Department of Physics at the university Abu Bekr Belkaid Tlemcen for accepting to chair my thesis defense and for the interest shown in this work.

My sincere thanks are also addressed to **Dr. Boufatah Mohammed Reda**, Examiner, Associate Professor in the Department of Physics at the university Abu Bekr Belkaid Tlemcen for kindly accepting to evaluate this work and for their valuable comments, suggestions, and constructive criticism, which have contributed to improving the quality of this thesis.

I would not forget to extend my thanks to the members of the Plasma Physics Research Group, the laboratory director Professor Bedrane Zeyneb, and the laboratory engineers Houda and Yahia

Dedication

I dedicate this work first and foremost to my beloved parents, whose endless love, sacrifices, and constant encouragement have been the foundation of my success and perseverance throughout my academic journey.

I dedicate this work to my supervisor, **Dr. Senoudi Assia Rachida**, for her unwavering support, patience, and guidance, and for standing by me step by step throughout this research.

I dedicate this work to my family for believing me everyone who supported me, even with a kind word, throughout this journey

Table Contents:

General Introduction

The generation of vapor nanobubbles around gold nanoparticles, induced by ultrashort laser pulses, produces a localized and controllable nanocavitation phenomenon. This has attracted considerable scientific interest owing to its potential applications in diverse fields, including photothermal therapy, nanosurgery, microfluidics, and materials processing. Nanocavitation is also relevant to surface cleaning processes.

The dynamics of nanocavitation are fundamentally governed by the interplay of multiple physical mechanisms, optics, thermal physics, mechanics, hydrodynamics, and thermodynamics. These phenomena all occur on extremely small spatial scales and ultrashort time scales.

Gold nanoparticles are generally placed in an aqueous solvant such as water or placed in a dielectric medium. The key aspect of the interaction between ultrashort laser pulses and gold nanoparticles lies in their ultrafast optical and thermal response. The optical response is characterized by strong light absorption in the visible and near-infrared ranges, followed by a localized and rapid thermal dynamics within the nanoparticle.

When subjected to ultrashort laser pulses, the energy absorbed by the gold nanoparticle is initially transferred to the electron system, leading to a rapid rise in electron temperature. To return to equilibrium, the electrons transfer their energy to the lattice through electron-phonon coupling, causing a further increase in the nanoparticle temperature. The nanoparticle then releases heat to the surrounding medium, a process particularly pronounced under femtosecond laser excitation, where the deposited energy density can be very high. This thermal dynamic takes place on a picosecond timescale. The resulting heat transfer to the surrounding medium can induce phase transitions, leading to explosive vaporization and nanocavitation in the form of vapor nanobubbles around the nanoparticle.

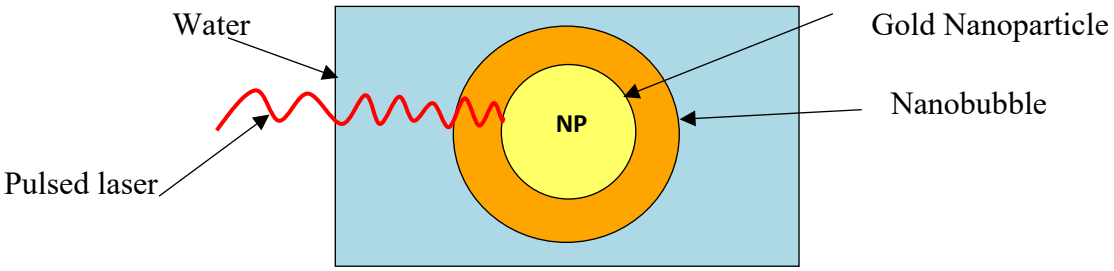

This work aims to establish a theoretical and numerical model based on three physical frameworks: the optical response of the nanoparticle, the thermal dynamics within the particle, and nanocavitation around the nanoparticle. The optical behavior of gold is described through an accurate characterization of its dielectric function, using a dipolar approximation well suited to the nanoparticle size. The thermal behavior is modeled using a framework specifically adapted to the ultrashort regime — femtosecond, picosecond, and nanosecond. For cavitation, a classical model is adopted to describe the nanobubble dynamics, assuming spherical symmetry.

The objective is to describe and analyze cavitation around the nanoparticle by simulating bubble growth and collapse. A single spherical nanoparticle subjected to a single Gaussian pulse of femtosecond duration is considered.

This work is organized as follows:

Chapter I is divided into two main sections. The first presents the properties of gold nanoparticles, focusing on their optical and thermal characteristics.
The optical properties describe the response of nanoparticles to light irradiation in the visible and near-visible range. The key quantities are the absorption and scattering cross-sections, which depend on the permittivity of the surrounding medium and the dielectric function of the metal at the confinement scale. Two standard models describing the dielectric function as a function of optical frequency are introduced for comparison with experimental data: the Drude model and the Drude model with Critical Points (DCP).
Since the particle size is very small compared to the wavelength of the incident field, the quasi-static (dipolar) approximation is used to calculate the optical cross-sections.
When subjected to femtosecond pulsed laser excitation, gold nanoparticles undergo ultrafast thermal dynamics in which the temperatures of two coupled subsystems, electrons and phonons change on a picosecond timescale. This is described by the Two-Temperature Model (TTM), whose equations and parameters are presented in detail.
The pulsed laser source is described through its main characteristics: the Gaussian temporal profile, pulse duration, and laser fluence.

Chapter II introduces the principle of phase change, the formation of cavitation bubbles, and the mathematical model describing the growth of a nanobubble radius as a function of time, namely the Rayleigh–Plesset equation. This equation involves characteristic hydrodynamic quantities and Thermodynamic quantities, in particular the vapor pressure, of the surrounding medium, water in the present case. We detail how the second-order differential equation is reduced to a system of first-order equations suitable for numerical integration.
The complete form of the equation requires knowledge of the vapor pressure inside the bubble. For this purpose, we adopt the standard Clausius–Clapeyron model, which gives the vapor pressure as a function of temperature. The nucleation threshold is defined by the temperature at the gold nanoparticle/water interface: when this interfacial temperature reaches the critical nucleation value, cavitation is initiated in the surrounding medium.

Chapter III: resents the obtained results of the simulations and their discussion.

This work required the development of a Python code modeling two coupled processes: the thermal dynamics (TTM) and the cavitation bubble growth and collapse (Rayleigh–Plesset equation).

The Python code I wrote requires Python 3.13 and the NumPy, Matplotlib, and SciPy libraries. The program was designed and implemented without the use of AI assistance.

Chapter One: General Overview of Gold Nanoparticles and Ultrafast Pulsed Laser

1.1 Introduction

Gold nanoparticles (AuNPs) have attracted considerable interest due to their unique optical and thermal properties also others physical properties. Their interaction with electromagnetic radiation, particularly through localized surface Plasmon resonance (LSPR), makes them highly relevant for a wide range of applications. This chapter is divided into two main sections:

- The first section provides a general overview of gold nanoparticles, including their synthesis using the Turkevich method, as well as their optical and thermal properties. The optical properties are described using the Drude and Drude–Lorentz models, while the thermal dynamic is analyzed using the two-temperature model (TTM).

- The second section focuses on pulsed lasers, with particular emphasis on femtosecond lasers, their fundamental principles, and operating mechanisms. It also presents the main characteristics of laser pulses and their mathematical description, especially the Gaussian pulse profile commonly used to model ultrashort pulses.

Since the present work deals with a multiphysics problem, this chapter provides only the basic elements required for the construction of the studied system, namely laser-induced cavitation. The discussion is limited to the key physical ingredients needed for the model formulation, including the optical response of the medium, thermophotonic models, and femtosecond pulsed laser excitation.

1.2 Gold nanoparticles

Gold nanoparticles are nanoscale noble metal, with dimensions typically ranging from 1 to 100 nanometers (1 nm = 10^{-9} m) in all spatial directions. They consist of a number of atoms varying from tens to several millions, depending on their size [1].

Gold is considered a unique element in the periodic table due to its high electron density, remarkable chemical stability, and distinctive color. It is also classified as a chemically inert metal, as it exhibits strong resistance to oxidation under normal conditions.

The chemical symbol of gold is (Au), and it has an atomic number of 79 and an atomic mass of 196.967 atomic mass units. It crystallizes in a face-centered cubic (fcc) structure and possesses a stable electron configuration given by: [Xe] $4f^{14}$ $5d^{10}$ $6s^{1}$. These intrinsic properties have contributed significantly to its importance throughout human history [2].

In recent years, interest in gold has increased considerably, particularly due to advances in the synthesis of gold nanoparticles and their wide range of applications in science and technology.

1.2.1 Synthesis of Gold Nanoparticles

There are two primary approaches for the synthesis of gold nanoparticles (**Figure 1.1**):

- ***Top-down approach:*** This method relies on the use of physical techniques to break down bulk materials into nanoscale particles. It involves reducing a macroscopic material into smaller structures until nanoparticles are obtained [3].
- ***Bottom-up approach:*** This is the most commonly used method for producing large quantities of gold nanoparticles. It is based on the assembly or aggregation of atoms or molecules to form nanoparticles. This approach is generally preferred over the top-down method due to its higher efficiency in production and the relative ease of controlling the size, shape, and surface properties of the nanoparticles [3].

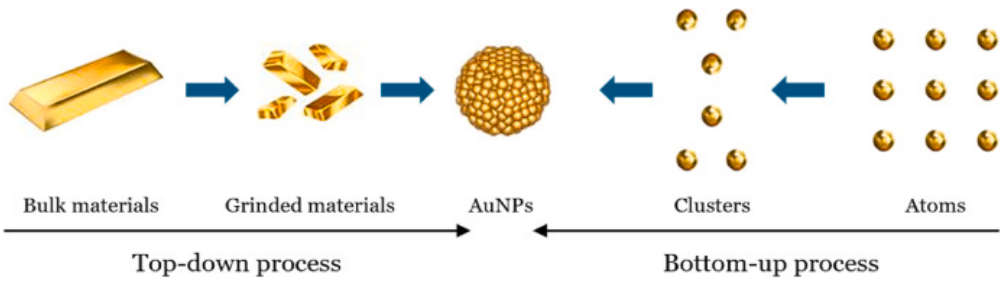

Figure 1.1: The two main methods for synthesizing gold nanoparticles [1]

Both the top-down and bottom-up approaches involve a variety of techniques, including physical, chemical, and biological methods for the synthesis of nanoparticles.

Table 1.1: Methods for synthesis of gold nanoparticles [1-3]:

Typical methods for the synthesis of gold nanoparticles		
Bottom-up approach		Top-down approach
Chemical Method	Biological Method	Physical Method
Turkevich method Brust Brust–Schiffrin method Digestive ripening Seed-mediated growth Citrate reduction synthesis	Microorganism Plants Biomolecule-mediated.	Microwave Laser ablation Irradiation techniques Sputtering Thermal decomposition.

The chemical synthesis of gold nanoparticles is one of the oldest and most widely used methods for producing metallic nanoparticles. Notably, Michael Faraday was among the first scientists to use chemical reduction processes to synthesize colloidal gold nanoparticles.

Among the various and recent chemical methods, the Turkevich method [4] **(Figure 1.2)** is the most commonly used. It is based on the reduction of gold salt (*Hydrogen Tetrachloroaurate* : $HAuCl_4$) using sodium citrate in an aqueous solution at its boiling point. The ratio between the concentrations of gold salt and sodium citrate plays a crucial role in controlling the size of the resulting nanoparticles, as later refined by Georges Frens [5,6]. During the reduction process, gold ions are converted into gold atoms (monomers), which rapidly accumulate until a state of supersaturation is reached. Once a critical concentration is exceeded, rapid nucleation occurs. Subsequently, the concentration of free monomers decreases below the critical level, leading to the cessation of nucleation. The final nanoparticles are then formed through the growth of the remaining monomers onto the already formed nuclei [6].

The technical methods for synthesizing gold nanoparticles allow control over their **size** , **shape** and **the surrounding environment**, making it possible to create particles of different sizes and shapes (**Figure 1.3)** with distinct optical and chemical properties.

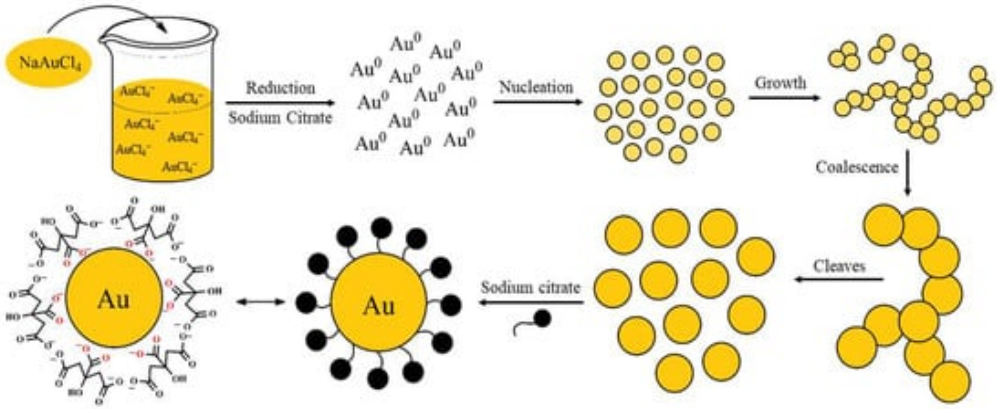

Figure 1.2: Schematic representation of synthesis of gold nanoparticles by Turkevich method [6].

At the nanoscale, the surface-to-volume ratio of gold nanoparticles increases significantly due to the higher proportion of surface atoms. This enhancement strongly influences their physical and chemical properties. Moreover, the surface can be readily functionalized with various biological molecules, making gold nanoparticles highly suitable for a wide range of applications across different scientific and technological fields.

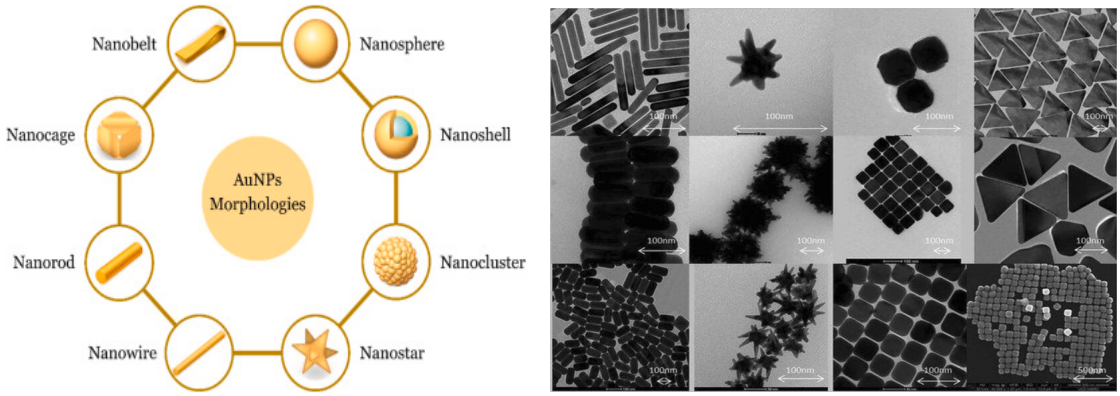

Figure 1.3 : Several geometric shapes of gold nanoparticles [1] (in left).
SEM micrographs of gold nanoparticles (in right) [7].

1.2.2 Properties of gold nanoparticles

Gold nanoparticles have optical, thermal and chemical properties that differ from those of gold in its bulk form. These exceptional and amazing properties make them, a material for a wide range of applications:

- ***Medicine and Biology:*** Gold nanoparticles are among the most important materials in medicine and biology due to their nanoscale dimensions, which allow them to interact efficiently with biological systems, including cancer cells (**Figure 1.3**). They are used for several biomedical applications:

Therapeutic agents can be efficiently conjugated to the surface of gold nanoparticles via electrostatic interactions or ligand receptor binding. Once internalized by target cells, the nanoparticles can release the drug payload selectively, thereby minimizing damage to healthy tissues. In addition, antibodies functionalized on gold nanoparticles enable the selective detection of cancer cells [8].

- ***In photothermal therapy***, gold nanoparticles accumulate in tumor tissues and are subsequently irradiated with light. They absorb the incident radiation and convert it into heat, leading to localized hyperthermia and destruction of cancer cells [9,10].
- ***Chemistry and Catalysis:*** AuNps exhibit enhanced catalytic activity due to their high surface-to-volume ratio and unique surface electronic structure. They are widely used in oxidation reactions, such as CO oxidation, and play an important role in green chemistry applications [11] .
- ***Electronics:*** Gold nanoparticles improve electrical conductivity in electronic devices by forming conductive networks between components. They are considered promising materials for flexible electronics, wearable devices, and high-performance sensing platforms [12].
- ***Solar Energy and Photothermal Conversion:*** AuNPs enhance solar absorption via plasmonic heating, improving thermal and photovoltaic conversion in solar collectors and hybrid nanofluids [13].
- ***Environment:*** AuNPs are employed in the detection and removal of heavy metal ions and pollutants from water and environmental remediation applications.

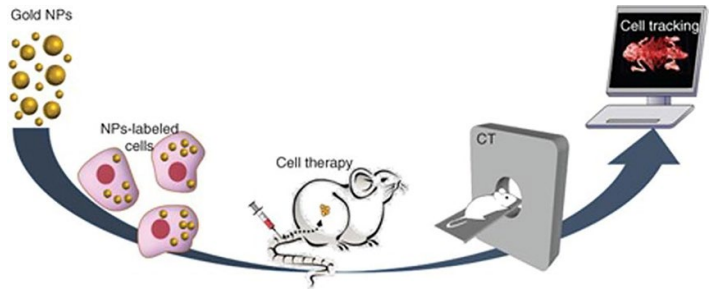

Figure 1.4 : Optical and Electron Microscopy Probing Using Gold Nanoparticles [14].

1. Optical properties

The optical properties of gold nanoparticles arise from the interaction between incident light and their free conduction electrons. When an electromagnetic field is applied, the oscillating electric field induces a collective displacement of these electrons relative to the positively charged ionic lattice, leading to the formation of an induced dipole. Under the influence of the restoring force, the electrons oscillate around their equilibrium position at a characteristic frequency known as the plasmon resonance frequency [15]. This phenomenon is referred to as localized surface plasmon resonance (LSPR) [16].

The plasmon resonance frequency of gold nanoparticles depends on particle size, shape, the dielectric properties of the surrounding medium, and interparticle coupling effects. By controlling these parameters, the optical response of gold nanoparticles can be tuned across the visible spectrum [17,18].

While bulk gold exhibits a characteristic yellow color, this optical property changes significantly at the nanoscale.

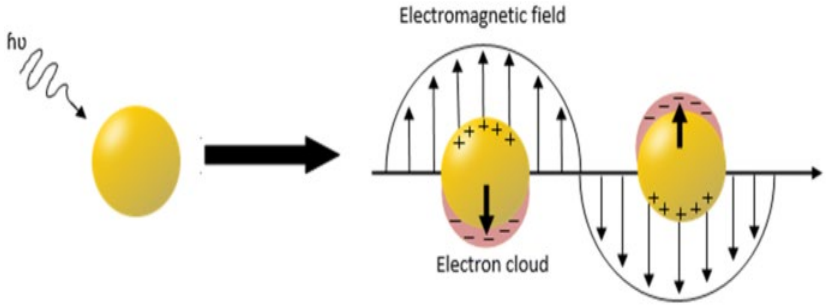

Figure 1.5 : Schematic representation of the localized plasmon resonance(LRSP)[17].

Colloidal solutions of gold nanoparticles display a range of colors, from red to blue, depending mainly on particle size, shape, and aggregation state [3].

Figure 1.6 : Effect of gold nanoparticle size on the apparent color of colloidal solutions [19].

a. ***Plasmonic effect***

When light is incident on nanoparticles, part of its energy is either absorbed by the particles or scattered in different directions.

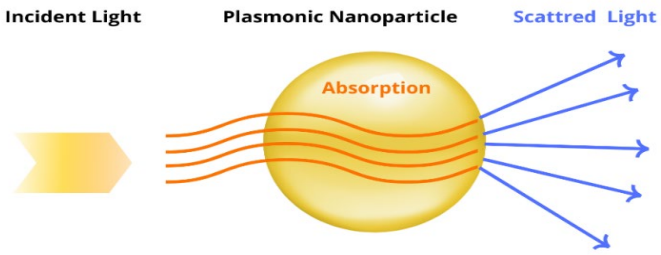

Figure 1.7: Light absorption and scattering in plasmatic nanoparticles.

Absorption: This phenomenon occurs due to the interaction between incident electromagnetic radiation and the conduction electrons of the nanoparticle, resulting in the conversion of part of the light energy into other forms, typically heat within the gold nanoparticle [20].

The efficiency of this process is described by the effective absorption cross-section σ_{abs}, defined as the ratio of the power absorbed by the gold nanoparticle P_{abs} to the intensity of the incident light I_0.

$$\sigma_{abs} = \frac{P_{abs}}{I_0} \tag{1.1}$$

Scattering: This phenomenon results by the generation of an oscillating electric dipole that re-emits light in all directions. A portion of the incident light is redirected without energy dissipation [21]. The efficiency of this process is described by the effective scattering cross-section σ_{sca}, defined as the ratio of the power scattered by the gold nanoparticle P_{sca} to the intensity of the incident light I_0 :

$$\sigma_{sca} = \frac{P_{sca}}{I_0} \tag{1.2}$$

An increase in the effective scattering cross-section corresponds to an increase in the intensity of light scattered by the nanoparticle, and conversely, a decrease in scattering cross-section leads to lower scattered intensity.

The effective extinction cross-section σ_{ext} is defined as the sum of the effective absorption σ_{abs} and scattering σ_{sca} cross-sections, representing the total attenuation of light energy due to the interaction with the nanoparticle:

$$\sigma_{ext} = \frac{P_{abs} + P_{sca}}{I_0} = \sigma_{abs} + \sigma_{sca} \quad (1.3)$$

b. ***Dielectric function***

The dielectric function or permittivity, namely ε(ω) is a fundamental physical parameter that describes how a material responds to an incident electromagnetic field. For noble metals such as gold, silver, and copper, this response arises from two main contributions:

- *Contribution of intraband transitions* ε^f : This term describes the response of free conduction electrons, involving electronic excitations within the same energy band. It is commonly modeled using the Drude model, which accounts for the motion of free electrons under an external electromagnetic field.
- *Contribution of interband transitions* ε^b **:** This term corresponds to electronic transitions between occupied states in the valence band and unoccupied states in the conduction band. We can express the dielectric function as the sum of these two contributions:

$$\varepsilon(\omega) = \varepsilon^f(\omega) + \varepsilon^b(\omega) \quad (1.4)$$

The intraband term $\varepsilon^f(\omega)$ is described by the classical Drude model, which was introduced by Paul Drude in 1908 and is based on a classical free electron approach in a plasma (kinetic theory of gas) [22] .

c. ***Classical Drude Model***

If an oscillating electric field $\vec{E}(t) = \vec{E}_0\, e^{i\omega t}$ is applied to a metal, such as gold, the free electrons will oscillate around their equilibrium position $\vec{r}$. Newton's second law describes the movement of the electron:

$$\vec{F} = m_{eff}\, \vec{a} = m_{eff} \frac{d^2\vec{r}}{dt^2} \quad (1.5)$$

where $\vec{r}$ represents the displacement from the equilibrium position and m_{eff} is the effective mass of electron.

The electric force applied to the electric field is given by:

$$\vec{F}_E = -e\, \vec{E}(t) \quad (1.6)$$

Electrons also experience collisions with surrounding particles, resulting in energy dissipation that can be modeled by a damping force given by:

$$\vec{F}_d = -m_{eff}\gamma\frac{d\vec{r}}{dt} \tag{1.7}$$

γ is the viscous damping coefficient, which depends on the mean free path $\tilde{\ell}$ and the Fermi velocity of the conduction electrons v_f equal to $\gamma = v_f / \tilde{\ell}$.

The sum of the forces (eqs 1.6 and 1.7) applied in eq. (1.5) leads to the equation of motion:

$$m_{eff}\frac{d^2\vec{r}}{dt^2} + m_{eff}\gamma\frac{d\vec{r}}{dt} = -e\,\vec{E}(t) \tag{1.8}$$

After derivation and simplification, we obtain the solution:

$$\vec{r}(t) = \frac{e}{m_{eff}(\omega^2 + i\omega\gamma)}\vec{E}(t) \tag{1.9}$$

This charge displacement will create macroscopic polarization, which is related to the dielectric function:

$$\vec{P}(\omega) = \varepsilon_0(\varepsilon^f(\omega) - 1)\vec{E}(t) \tag{1.10}$$

where ε_0 is the permittivity of vacuum.

$$\vec{P}(\omega) = -n_e\vec{r}\,\vec{E}(t) = -\frac{n_e e^2}{m_{eff}(\omega^2 + i\omega\gamma)}\overrightarrow{E}(t) \tag{1.11}$$

By identification between (1.10) and (1.11), we obtain Drude's dielectric function:

$$\varepsilon^f(\omega) = 1 + \frac{n_e e^2}{\varepsilon_0\, m_{eff}(\omega^2 + i\omega\gamma)} = 1 + \frac{\omega_p^2}{(\omega^2 + i\omega\gamma)} \tag{1.12}$$

with, $\omega_p = \sqrt{\frac{n_e e^2}{\varepsilon_0 m_{eff}}}$, the plasma frequency, n_e the density of electrons and e the elementary charge. The dielectric function associated with intraband transitions can be expressed in terms of its real and imaginary parts as follows:

$$\varepsilon^f(\omega) = \varepsilon_1(\omega) + i\varepsilon_2(\omega) \tag{1.13}$$

For extremely high frequencies, the first term of Drude in (1.12) must be corrected to match the experimental data. This is achieved by improving it based on the contribution of bound electrons. The modified Drude model is then written as:

$$\varepsilon_1(\omega) = \varepsilon_\infty - \frac{\omega_p^2}{(\omega^2 + \gamma^2)} \tag{1.14}$$

$$\varepsilon_2(\omega) = \frac{\omega_p^2 \gamma}{\omega(\omega^2 + \gamma^2)} \tag{1.15}$$

ε_∞ represents the contribution of bound electrons at high frequencies.

The confinement effects can significantly modify the dielectric function of metallic nanoparticles. When the particle size decreases, the surface-to-volume ratio increases, leading to more frequent electron–surface collisions. As a result, the total collision rate becomes higher than in the bulk material. These size dependent effects are incorporated into the Drude model by introducing a corrected damping term:

$$\tilde{\gamma}(D) = \gamma + \frac{v_f}{L} \tag{1.16}$$

where $\tilde{\gamma}$ is the collision rates of confined metal, L is the effective mean free path of collisions with the surface.

Table 1.2: Parameters of Drude Model [23].

Material parameters	**Value**
ε_∞	9,8
e (c)	$1{,}6 \times 10^{-19}$
n_e (m^{-3})	$5{,}9 \times 10^{28}$
m (kg)	$9{,}1 \times 10^{-31}$
m_{eff} (kg)	$m \times 0{,}99$
ε_0	$8{,}85418782 \times 10^{-12}$
ω_p (eV)	9,03
γ (eV)	0,07

The dielectric function of Drude model and Drude modified model is plotted as a function of wavelength in (nm) and is compared to the experimental data of Johnson and Christy (JC) [24]. The corresponding plots can be found in **Figure 1.8.**

These results are obtained through the personnel Python code which implement the Drude (1.12) and Drude modified model (1.14-1.15).

Code Python: Dielectric function of AuNP: Drude Models:

```
import numpy as np
import matplotlib.pyplot as plt
wp = 9.03        , gamma = 0.07  , epsilon_inf = 9.8   , N = 200
lambda_ = []
w = []
epsilon  = []
epsilon1 = []
epsilon2 = []
for i in range(N):
    lam = 200 + i*10
    w = 1236.37/lam
    epsilon = epsilon_inf - wp**2/(w**2 + 1j*gamma)
    eps1 = epsilon.real
    eps2 = epsilon.imag
    lambda_.append(lam)
    epsilon1.append(eps1)
    epsilon2.append(eps2)
    file = open("Drude_Mod.dat","w")
for i in range(N):
    file.write("{:10.2f} {:15.6f} {:15.6f}\n".format(lambda_[i], epsilon1[i],
epsilon2[i]))
file.close()
# trace
plt.figure()
plt.plot(lambda_, epsilon1)
plt.xlabel("lambda (nm)")
plt.ylabel("epsilon1")
plt.title("Real part of dielectric function")
plt.figure()
plt.plot(lambda_, epsilon2)
plt.xlabel("lambda (nm)")
plt.ylabel("epsilon2")
plt.title("Imaginary part of dielectric function")
plt.show()
```

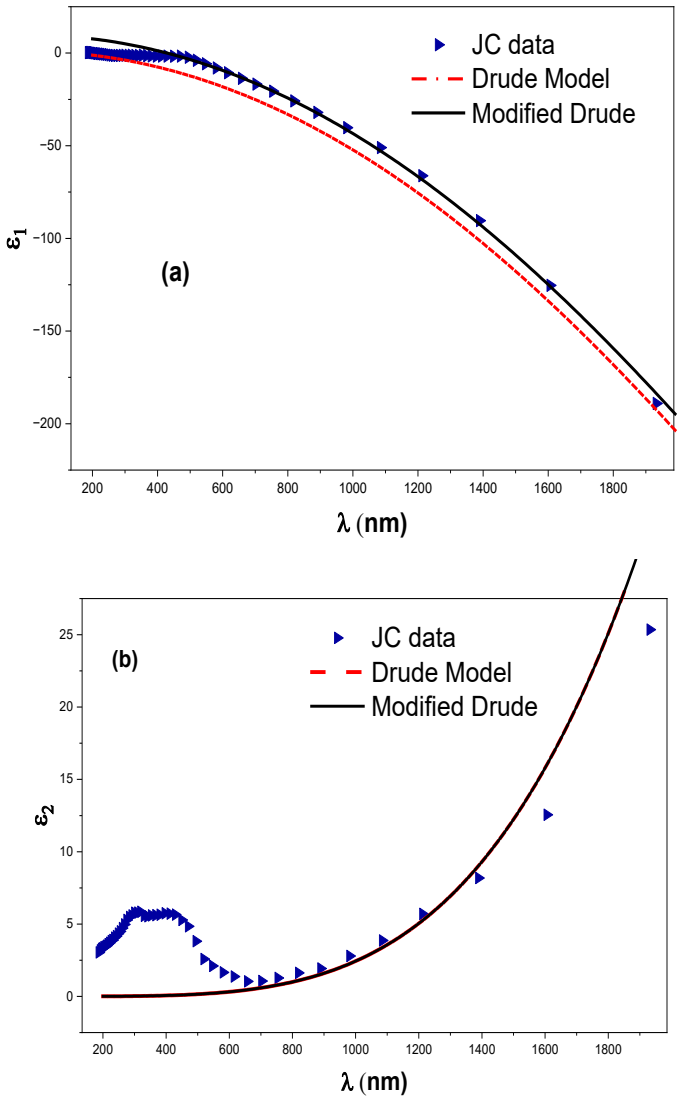

Figure 1.8 : : Dielectric function, real part (a) and imaginary part (b), based on the Drude model (red dotted line), the modified Drude model (black solid line) and the measurements by Johnson and Christy (blue triangle).

Conclusion: *The Drude model primarily describes the response of free conduction electrons and is therefore valid only within a limited spectral range where their contribution dominates, as confirmed by the experimental data of Peter B. Johnson and R. W. Christy. However, at short wavelengths, the model fails due to the increasing importance of interband transitions involving bound electrons, leading to deviations from experimental results. Consequently, more advanced models, such as the Drude–Lorentz model, are required to accurately account for both free and bound electron contributions.*

d. Lorentz Model

In order to accurately describe the optical response of metals over a wide frequency range, it is necessary to consider both free-electron and bound-electron contributions. To achieve this, the Drude model is commonly extended by incorporating additional terms known as Lorentz oscillators [25] , which account for interband transitions:

$$\varepsilon(\omega) = \varepsilon_\infty - \frac{\omega_D^2}{\omega(\omega + i\gamma)} + \sum_{l=1}^{2} \frac{f_l \ \Omega_l^2}{\Omega_l^2 \ - \omega^2 \ - i\Gamma_l \, \omega} \tag{1.17}$$

Ω_l: the resonant frequencies of the oscillator, Γ_l : the resonant bandwidths in the Drude Lorentz model, and the coefficients f_l give the measure of the probability that a transition will occur at frequency Ω_l.

Table 1.3: Parameters of Lorentz Model [26].

Material parameters	**Value**
ε_∞	6,2137
$\omega_D(\mathrm{eV})$	8,7432
$\gamma(\mathrm{eV})$	0,0868
f_1	3,4620
$\Omega_1(\mathrm{eV})$	3,1443
$\Gamma_1(\mathrm{eV})$	1,4022
f_2	-3,488
$\Omega_2(\mathrm{eV})$	27,635
$\Gamma_2(\mathrm{eV})$	299,06

The dielectric function of gold is modelled using the Drude-Lorentz model and compared with the experimental data of Johnson and Christy (JC) [24]. The corresponding plots can be found in **Figure 1.9** .and we present the Python code developed to implement the Drude-Lorentz model.

Code Python: Dielectric function of AuNP: Lorentz Model.

```
import numpy as np
import matplotlib.pyplot as plt
wd=8.7432
gamma=0.0868
eps_inf=6.2137
f1=3.4620
f2=-3.488
w1=3.1443
w2=27.635
gamma1=1.4022
gamma2=299.06
N=200
lambda_=[]
epsilon1=[]
epsilon2=[]
for i in range(N):
    lam=200+i*10
    w=1236.37/lam
    # Drude Modified term
    epsdrude =eps_inf-wd**2/(w**2+1j*gamma*w)
    # Lorentz term
    epsL1=f1*w1**2/(w1**2-w**2-1j*gamma1*w)
    epsL2=f2*w2**2/(w2**2-w**2-1j*gamma1*w)
    epsL=epsL1+epsL2
    # Total dielectric function
    epsilon=epsdrude+epsL
    eps1=epsilon.real
    eps2=epsilon.imag
    lambda_.append(lam)
    epsilon1.append(eps1)
    epsilon2.append(eps2)
    file = open("Lorenyz.dat","w")
for i in range(N):
    file.write("{:10.2f} {:15.6f} {:15.6f}\n".format(lambda_[i], epsilon1[i], epsilon2[i]))
file.close()
# trace
plt.figure()
plt.plot(lambda_, epsilon1 )
plt.xlabel("lambda (nm)")
plt.ylabel("epsilon1")
plt.title("Real part of dielectric function")
plt.figure()
plt.plot(lambda_, epsilon2)
plt.xlabel("lambda (nm)")
plt.ylabel("epsilon2")
plt.title("Imaginary part of dielectric function")
plt.show()
```

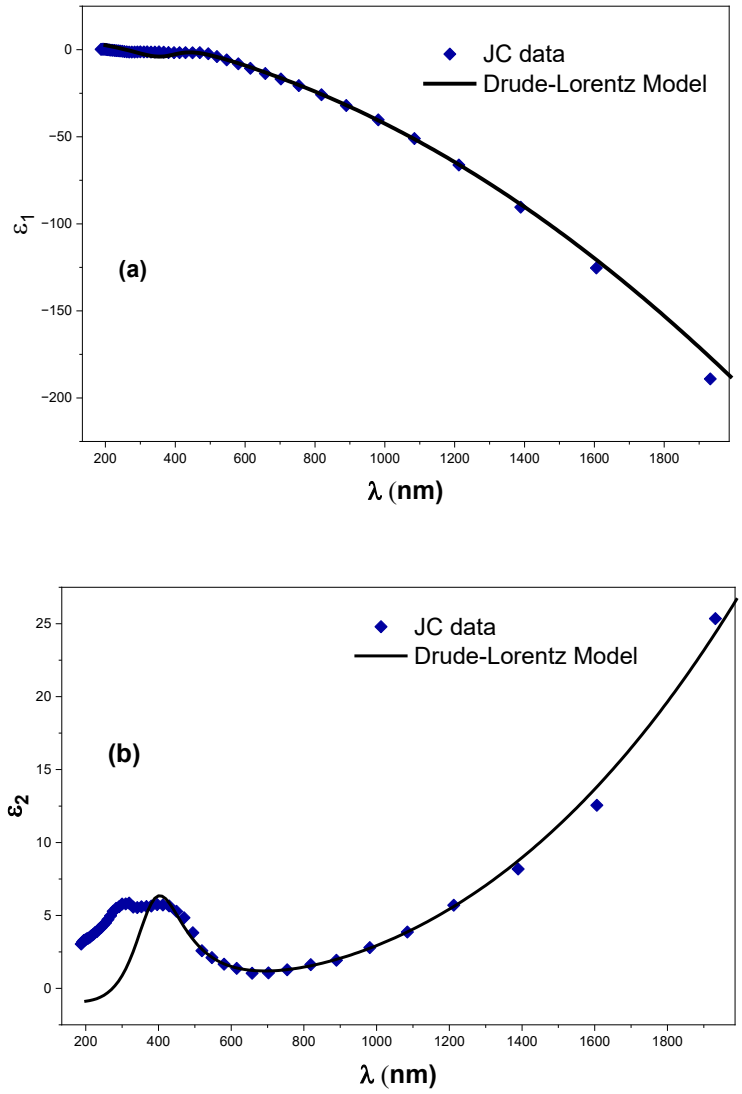

Figure 1.9: Dielectric function, real part (a) and imaginary part (b), based on the Drude-Lorentz model (black solid line) and the measurements by Johnson and Christy (blue square).

After determining the dielectric function of gold using the Drude model and subsequently the Lorentz model, we proceed to the calculation of the different optical cross-sections. These quantities are essential for characterizing the interaction of light with the material and for analyzing its optical response under various conditions.

e. The quasi-static approximation

We consider a metallic spherical nanoparticle of volume V, characterized by a complex dielectric function $\varepsilon(\omega) = \varepsilon_1(\omega) + i\varepsilon_2(\omega)$ and embedded in a homogeneous, non-absorbing dielectric medium with dielectric constant:

$$\varepsilon_m = {n_m}^2 \tag{1.18}$$

where n_m is the refractive index of the surrounding medium.

The quasi-static approximation is used to describe the interaction between a nanoparticle and an electromagnetic wave when the particle diameter is much smaller than the wavelength (D ≪ λ). Under this condition, the spatial variation of the electric field can be ignored, and the nanoparticle is modeled as an electric dipole subjected to a uniform external field $\vec{E}$ [27].

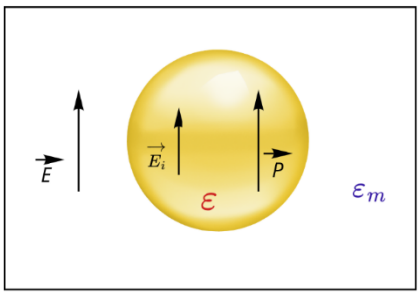

Figure 1.9: Schematic representation of a spherical metallic nanoparticle with permittivity ε, embedded in a dielectric medium of permittivity ε_m, and subjected to an external electric field $\vec{E}$.

When a gold nanoparticle is subjected to an external electric field $\vec{E}$, it develops a dipole moment that is linearly related to the field. This relationship is determined by the particle's polarizability α, and can be mathematically [28] written as:

$$\vec{p} = \varepsilon_0 \varepsilon_m \alpha \vec{E} \tag{1.19}$$

For a density of dipoles N per unit volume, the macroscopic polarization is:

$$\vec{P} = N\vec{p} = N\varepsilon_0 \varepsilon_m \alpha \vec{E} \tag{1.20}$$

The static depolarization field at the center of a uniformly polarized nanoparticle [28] is:

$$\vec{E}_{dep} = -\frac{\vec{P}}{3\,\varepsilon_0 \varepsilon_m} \tag{1.21}$$

The negative sign indicates that the depolarization field opposes the polarization. The total internal field $\vec{E}_i$ inside the nanoparticle is the sum of the local field and the depolarization field:

$$\vec{E}_i = \vec{E} + \vec{E}_{dep} \tag{1.22}$$

By substitution of (1.21) in (1.22):

$$\vec{E}_i = \vec{E} - \frac{\vec{P}}{3\,\varepsilon_0 \varepsilon_m} \tag{1.23}$$

The macroscopic polarization and the internal field are related through the electric susceptibility, ξ [29]:

$$\vec{P} = \varepsilon_0 \xi \vec{E}_i \;\; = \varepsilon_0(\varepsilon - \varepsilon_m)\vec{E}_i \tag{1.24}$$

By substituting equations (1.24) into equation (1.23), we obtained the expression that relates the internal electric field to the local field:

$$\vec{E}_i = \left(\frac{3\varepsilon_m}{\varepsilon + 2\varepsilon_m}\right)\vec{E} \tag{1.25}$$

By replacing this last expression of internal field in eq. (1.24), the following expression is obtained:

$$\vec{P} = \varepsilon_0(\varepsilon - \varepsilon_m)\left(\frac{3\varepsilon_m}{\varepsilon + 2\varepsilon_m}\right)\vec{E} \tag{1.26}$$

By identification (1.26) with the expression (1.20), we obtain, the polarizability of spherical nanoparticle:

$$N\alpha = 3\left(\frac{\varepsilon - \varepsilon_m}{\varepsilon + 2\varepsilon_m}\right) \tag{1.27}$$

In the case where the sphere is modeled as an equivalent single dipole, the dipole density is inversely proportional to the particle volume $N = \frac{1}{V}$. This assumption leads to,

$$\alpha = 3V\left(\frac{\varepsilon - \varepsilon_m}{\varepsilon + 2\varepsilon_m}\right) \tag{1.28}$$

The optical cross-sections can be found in terms of polarizability as reported in [20] as :

$$\sigma_{ext} = k\, Im[\alpha] = \frac{18V\pi {\varepsilon_m}^{1/2}}{\lambda}\frac{\varepsilon_2}{(\varepsilon_1 + 2\varepsilon_m)^2 + {\varepsilon_2}^2} \tag{1.29}$$

$$\sigma_{sca} = \frac{k^4}{6\pi}|\alpha|^2 = \frac{144V^2\pi^4 {\varepsilon_m}^2}{\lambda}\frac{(\varepsilon_{1-}\varepsilon_m)^2 + {\varepsilon_2}^2}{(\varepsilon_1 + 2\varepsilon_m)^2 + {\varepsilon_2}^2} \tag{1.30}$$

$$\sigma_{abs} = \sigma_{ext} - \sigma_{sca} \tag{1.31}$$

where k represents the wavelength vector:

$$k = \frac{2\pi n_m}{\lambda} = \frac{2\pi {\varepsilon_m}^{1/2}}{\lambda} \tag{1.32}$$

For small nanoparticles, the scattering intensity is very low [20,27]:

$$\sigma_{abs} \approx \sigma_{ext} \tag{1.33}$$

In addition to their optical properties, nanoparticles exhibit photothermal effects that are of particular interest; the basic principles of this thermos-heating phenomenon will be briefly discussed in the following section.

2. Thermal Dynamics

Understanding the thermal properties of a particle is essential for comprehending how it absorbs converts, and dissipates energy when exposed to external radiation [30]. two main types of excitations can be cited:

- Continuous and stable irradiation (e.g. continuous laser).
- Irradiation in the form of very short pulses (pulsed lasers).

Particular attention is given to pulsed lasers, as their ultrashort duration enables rapid excitation of free electrons before thermal equilibrium is established. Following the absorption of an ultrashort laser pulse, the thermal response of a metallic nanoparticle can be divided into four successive stages [31,32]:

Photon Absorption: When an ultrashort laser pulse interacts with a gold nanoparticle, the conduction electrons absorb part of the incident electromagnetic energy. This absorption leads to electron excitation and an increase in the electronic energy of the nanoparticle. In the case where, the excitation wavelength is close to the localized surface plasmon resonance (LSPR) wavelength, a strong plasmon excitation occurs, resulting in highly efficient energy transfer to the electron gas.

***Electron thermalization (e–e scattering)*:** Immediately after absorption, the electron distribution is in a non-equilibrium state because only a fraction of the electrons is directly excited. Through electron–electron (e–e) scattering, the absorbed energy is rapidly redistributed among the electron population, leading to the formation of a thermalized electron gas characterized by an elevated electron temperature (T_e). This process typically occurs within a few tens to hundreds of femtoseconds.

***Electron-phonon interaction*:** The hot electrons subsequently transfer their energy to the crystal lattice through electron–phonon coupling. As a result, the lattice temperature

(T_L) increases while the electron temperature (T_e) decreases This energy exchange generally takes place on a picosecond timescale until thermal equilibrium is reached ($T_e = T_L$).

***Phonon–phonon interaction*:** Following electron–phonon equilibration, heat is transferred from the nanoparticle to the surrounding medium through phonon–phonon interactions and thermal diffusion. Consequently, the nanoparticle gradually cools while the temperature of the surrounding medium increases. This stage typically occurs on nanosecond timescales.

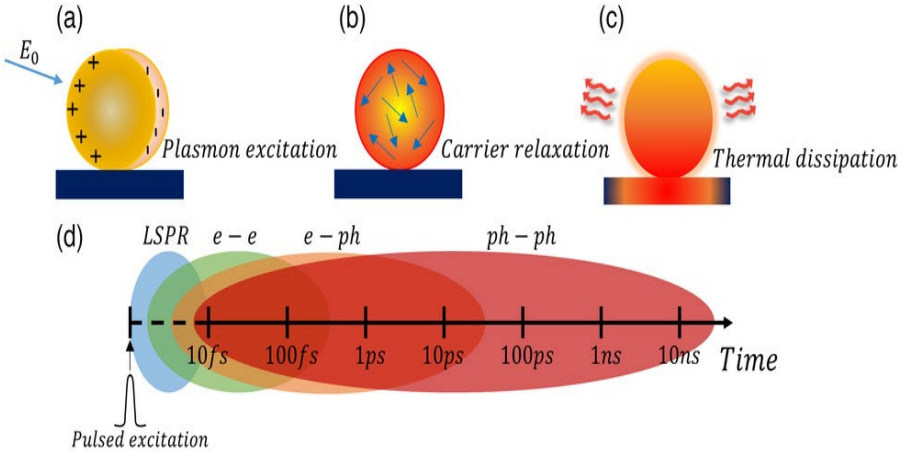

Figure 1.11 : Dynamics of Plasmon relaxation in gold nanoparticles [33].

Conclusion: *Under high pulsed laser irradiation, the rapid heating of gold nanoparticles can raise the local temperature of the surrounding medium beyond its boiling point, leading to the formation of vapor nanobubbles. These bubbles originate from efficient energy transfer from the excited electrons to the lattice and then to the surrounding medium. Their formation and dynamics (growth and collapse) occur on nanosecond timescales. This phenomenon is important in applications such as photothermal therapy and nanoscale manipulation.*

a. Heat equation Model

Upon irradiation by a pulsed laser, a nanoparticle absorbs electromagnetic energy, causing a rapid rise in its electron temperature. The absorbed energy is then converted into heat and redistributed within the nanoparticle through thermal diffusion.

The resulting heat transfer within the nanoparticle can be described by the heat diffusion equation. The temporal and spatial evolution of the temperature within the nanoparticle, T_{NP} [18], is governed by the heat diffusion equation:

$$C_{Au}\frac{\partial T_{NP}(\vec{r},t)}{\partial t} = \kappa_{Au}\nabla^2 T_{NP}(\vec{r},t) + P_{abs}(t) \qquad (1.34)$$

C_{Au} is the volumetric heat capacity of the particle, κ_{Au} is the thermal conductivity of the particle, ∇^2 is the second spatial derivative (Laplacian) which expresses the diffusion of heat in three-dimensional space, and P_{abs} (t) is the energy absorbed by the particle.

b. Two temperature Model (TTM)

The two-temperature model (TTM) is widely used to describe the ultrafast thermal dynamics of metallic nanoparticles. In this framework, the nanoparticle is represented by two coupled subsystems: an electron subsystem characterized by the electron temperature T_e and a lattice subsystem characterized by the lattice temperature T_L [34]. On ultrafast timescales, heat transfer to the surrounding medium is generally neglected, and the energy exchange occurs mainly between electrons and the lattice. The TTM model [35] is expressed as:

$$C_e(T_e)\frac{dT_e(t)}{dt} = -g(T_e - T_L) + S(t) \tag{1.35}$$

$$C_L(T_L)\frac{dT_L(t)}{dt} = g(T_e - T_L) \tag{1.36}$$

C_e is the thermal capacity of electrons by unit of volume, the term $g(T_e - T_L)$ represents the energy transferred from the electrons to the metal lattice by unit volume of the Np and by unit time, while S(t) corresponds to the energy source term generated in the nanoparticle by the laser pulse. C_L is the thermal capacity by unit of volume of the lattice, T_e and T_L are respectively the temperatures of the electrons and the metal lattice, g represents the electron-phonon coupling in thermal dynamics.

For metallic nanoparticles, the classical two-temperature model can be extended to include energy dissipation to the surrounding environment. Due to their high surface-to-volume ratio, the nanoparticle interface plays a crucial role in cooling, as heat is transferred from the lattice to the external medium .The thermal behavior of the system [36] can be described by :

$$C_e(T_e)\frac{dT_e(t)}{dt} = -g(T_e - T_L) + S(t) \tag{1.37}$$

$$C_L(T_L)\frac{dT_L(t)}{dt} = g(T_e - T_L) - Q \tag{1.38}$$

$$C_m(T_m)\frac{\partial T_m(\vec{r},t)}{\partial t} = \kappa_m \nabla^2 T_{\text{m}} + Q \tag{1.39}$$

where C_m is the heat capacity of the medium by unit of volume, T_m is the temperature of medium, κ_m is the thermal conductivity of the medium and Q is a term describing heat exchange at the NP interface with the external environment.

The Fourier's Law [37], gives the quantity of energy loosed through the surface S_P of the AuNP:

$$Q = \frac{S_P}{a}\int_{T_\infty}^{T} k(T)\, dT \tag{1.40}$$

where S_P and a are the surface area and the radius of the spherical gold nanoparticle, respectively. T_S is the temperature at the AuNp/water interface and T_∞ is the ambient water temperature, $k(T)$ represents the function of the thermal conductivity of water, which can be expressed as $k(T) = k_\infty \left(\frac{T}{T_\infty}\right)$ [38],with $k_\infty$is the thermal conductivity of water at $T_\infty = 300\ K$. Substituting the expression of $k(T)$ into equation (1.40) and calculating the integral, we find:

$$Q = 2\pi a k_\infty T_\infty \left(\left(\frac{T_L(t)}{T_\infty}\right)^2 - 1\right) \tag{1.41}$$

In next section, we introduce the basic principles of lasers and the fundamental characteristics of ultrafast laser systems.

1.3 Fundamentals of Pulsed Lasers

LASER is an acronym for "Light Amplification by Stimulated Emission of Radiation". Which is an optical system that converts energy into electromagnetic radiation in the form of a focused beam of light which is characterized by being monochromatic, highly collimated and coherent [39].

Albert Einstein discovered the phenomenon of stimulated emission in 1917, which forms the basis of laser operation. Between 1951 and 1954, the first maser device was developed, operating in the microwave range. Gordon Gould later introduced the term "laser". In 1960, Theodore Maiman built the first practical ruby laser. Following this breakthrough, several types of lasers were developed, including the helium–neon laser, CO_2 laser, Nd:YAG laser, diode lasers, and dye lasers [40] , enabling a wide range of applications in science and technology, including :

- ***Medicine:*** Laser technology is employed in a wide range of medical applications, playing a pivotal role in ophthalmology and vision correction. It is also utilized for the removal of tattoos and birthmarks through selective photo-thermolysis. Moreover, lasers are increasingly applied in oncology to eradicate cancerous cells via their interaction with gold nanoparticles [41,42] .

- ***Electronics:*** Lasers are employed in a variety of technological applications, including barcode scanning systems, laser printers, and projection devices. In these applications, optical signals are converted into digital information or visual images with high accuracy and efficiency [43].
- ***Manufacturing:*** Lasers can also be relied upon for metal cutting and welding due to their high precision, in addition to their application in the fabrication and cutting of three-dimensional models [44] .
- ***Measurement:*** Lasers are also employed in metrology techniques to measure distances and velocities with high precision, relying on the time-of-flight of light pulses or the Doppler effect. This makes them highly effective tools for both scientific and industrial applications.
- ***Communications:*** lasers are employed to transmit internet data through optical fibers in the form of laser pulses. This process can also involve three-dimensional mapping techniques based on LiDAR, and lasers are further utilized across various frequency bands for data transmission [45] .

1.3.1 Principle of laser functioning

A laser consists of three key components that enable it to propagate within an amplifying medium to produce a directional, monochromatic beam that is in coherence [46] :

- ***Active medium:*** This medium can be a solid (Ruby laser, Nd: YAG laser, and diode lasers), liquid (Rhodamine 6G laser) or gas (Helium–Neon laser, Co_2 laser). When a photon passes through it and interacts with an excited atom, the atom emits another photon with the same energy and in the same direction, this process is known as stimulated emission [48] .

- ***Optical Cavity:*** The active medium is placed inside a cavity formed by two mirrors, one fully reflective and the other partially reflective. These mirrors confine the radiation, allowing multiple passes through the medium, which leads to amplification, while a fraction of the light is transmitted as the laser output [48] .

- ***Pumping system:*** The pumping mechanism supplies the active medium with external energy to excite its atoms to higher energy levels, creating a population inversion necessary for laser operation. This energy can be provided by optical sources (such as another laser), electrical sources (such as electric discharge or laser diodes), or chemical processes [22].

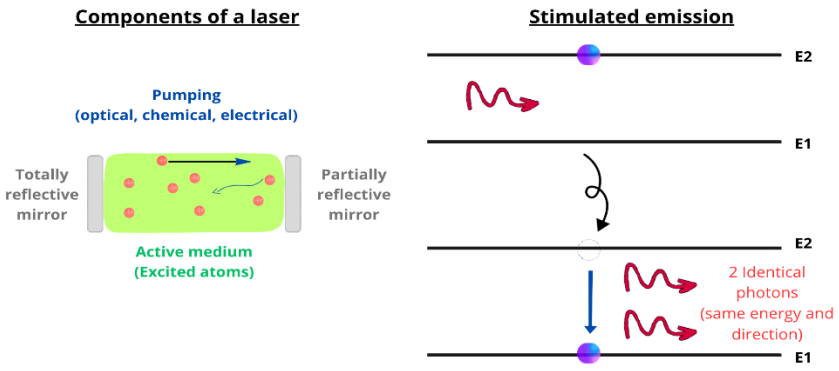

Figure 1.12: Principle of laser functioning (Left) and stimulated emission (Right).

1.3.2 Pulsed laser

There are two main types of lasers: three-level lasers, which typically operate in pulsed mode, and four-level lasers, which operate in continuous-wave mode. Pulsed lasers emit brief bursts of light, for which both the pulse duration and repetition rate can be controlled [49] .

Pulsed lasers are particularly suitable for a wide range of applications due to their ability to deliver energy to materials on extremely short timescales. Two categories are distinguished:

- Lasers with nanosecond pulses.
- Ultra short-pulse lasers with picosecond or femtosecond pulses

Because ultra-short laser pulses deliver energy to the material on a timescale much shorter than thermal diffusion, the initial response of metallic nanoparticles is governed by rapid electronic excitation, occurring before any significant lattice heating.

1. The different pulse regimes:

The interaction between the laser and the material depends on the duration of the laser pulse. For this reason, there are three main systems:

- ***The nanosecond regime*** **(ns)**: thermal effects dominate where the pulse duration is around 10^{-9} seconds, the interaction between the laser and the material. The absorbed energy is efficiently transferred from the electrons to the lattice, which can result in melting of the material [50] .

- ***Picosecond regime* (ps)*:*** The pulse duration about 10^{-12} seconds, the excited electrons begin interacting with the lattice, transferring energy and raising the lattice temperature. This electron–phonon coupling initiates the thermalization process within the material [50].

- ***Femtosecond regime* (fs)*:*** With pulse durations approximately 10^{-15} seconds, this regime is significantly faster than the nanosecond and picosecond regimes .In this timescale, electrons can absorb energy before significant heat is transferred to the lattice, making the interaction effectively non-thermal and enabling precise, high-quality material processing [50].

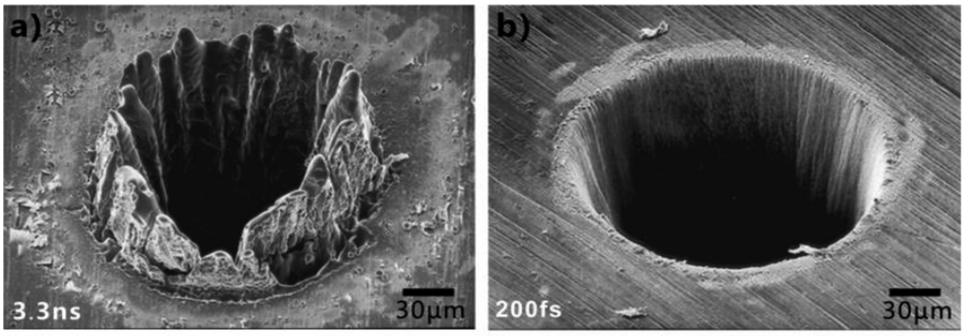

Figure 1.13: Results of ns-Laser–Material interaction (in Left) and results of fs-Laser–Material interaction (in Right) [51] .

A pulsed laser generates light pulses through the superposition of multiple longitudinal modes within its cavity. When these modes are phase-locked, the output signal becomes pulsed, a phenomenon referred to as mode locking. Every k mode has an electric field E_k and a mode frequency, ω_k given as:

$$\omega_k = \omega_0 + 2\pi k F_r \tag{1.42}$$

with F_r is the resonance frequencies and ω_0 frequency of fundamental mode.

The total electric field for all modes is given by:

$$E(t) = \sum_{k=0}^{N-1} E_k e^{-i\omega_k t} \tag{1.43}$$

N is the number of in-phase modes.

A simple mathematical calculation shows that the laser intensity, in case where all fields have the same amplitude E_0, is:

$$I(t) = |E(t)|^2 = {E_0}^2 \times \frac{\sin^2(N \times \frac{\omega t}{2})}{\sin^2(\frac{\omega t}{2})} \tag{1.44}$$

We evaluate the intensity $I(t)$ for two cases of phase-locked modes, N=5 and N=10 (as implemented in the Python code). For clarity, a typical value of the repetition rate is used $F_r = 15\ MHz$. In the simulation we set $E_0 = 1$. The obtained results are illustrated in Figure 1.14.

Code Python: Profile of the Laser Intensity.

```
import numpy as np
import matplotlib.pyplot as plt
fr = 15e6
omega = 2*np.pi*fr
# number of modes
N1 = 5
N2 = 10
file = open("intensity.dat","w")
# time (ns)
t = np.arange(-50,300,0.1)
t=t*1e-9
I1 = np.sin(N1*omega*t/2)**2/np.sin(omega*t/2)**2
I2 = np.sin(N2*omega*t/2)**2/np.sin(omega*t/2)**2
I2 = I2 + 30
for i in range(len(t)):
    file.write("%f %f %f\n"%(t[i]*1e9,I1[i],I2[i]))
file.close()
# trace
plt.plot(t*1e9, I2, label='N = 10 modes')
plt.plot(t*1e9, I1, label='N = 5 modes')
plt.xlabel("Time (ns)")
plt.ylabel("Light intensity")
plt.title("Pulse train generated by synchronized mode superposition")
plt.legend()
plt.grid()
plt.show()
```

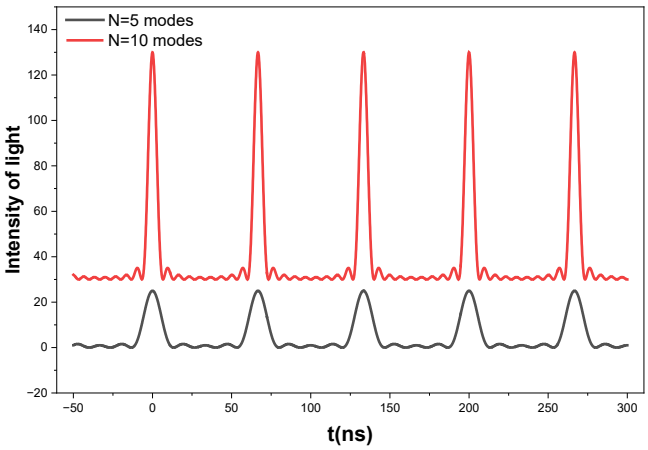

Figure 1.14: A train of pulses generated by the superposition of synchronized waves.

Figure 1.15 shows a single pulse obtained for $N = 5 \times 10^4$ and a repetition rate of $Fr = 100\,MHz$. From this figure, the pulse's full width at half maximum (FWHM) is clearly observed to be $\tau_p = 0.18\,ps = 180\,fs$.

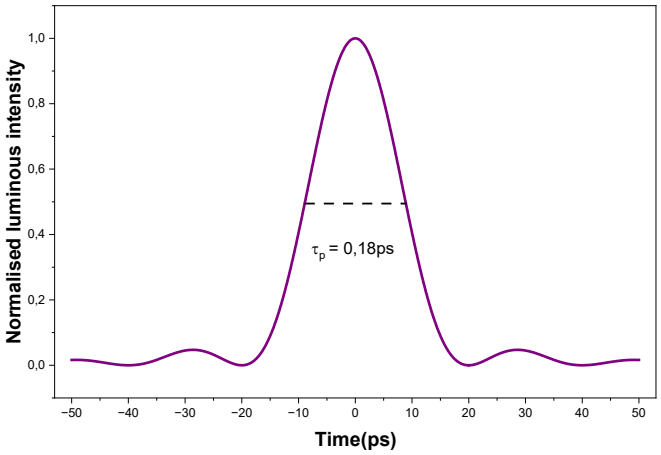

Figure 1.15: Femtosecond pulse.

Conclusion: *It is important to emphasize that increasing the number of phase-locked modes results in a reduction of the pulse duration. Analysis of the graphs indicates that the output of the laser exhibits a pulse-train structure, with each pulse arising from the coherent superposition of N synchronized modes. As the number of in-phase modes increases, both the pulse intensity rises and the pulse width decreases. Individual pulses can be accurately modeled using a Gaussian profile, and in a femtosecond laser, they are emitted at regular intervals.*

2. Characteristics of a Femtosecond Laser Pulse:

The following section presents the main characteristics of a pulsed laser.

- ***The pulse width τ_p*:** The full width at half maximum of the pulse intensity $(FWHM)^2$ is defined as the duration of the pulsed power measured at half of its maximum value, expressed in femtoseconds.
- ***Pulse Energy E*:** corresponds to the total energy emitted (P) during one pulse.

$$E = P \times \tau_p \tag{1.45}$$

- ***Wavelength (λ):*** related to the photon energy of the pulse laser.

$$\lambda = \frac{c}{\nu} \tag{1.46}$$

with, ν the frequency of the laser.

- ***Pulse Photon Number N:*** The total number of photons released during a single laser pulse, calculated from the pulse energy and photon energy.

$$N = \frac{E}{h\nu_0} \tag{1.47}$$

- ***Laser Fluence F:*** The energy delivered per unit area (A) by a single laser pulse, expressed in J/cm².

$$F = \frac{E}{A} \tag{1.48}$$

- ***Mathematical Model of a Single Femtosecond Pulse:*** For the purpose of studying laser–particle interactions and analyzing their temporal evolution, a single isolated pulse is considered instead of a pulse train. Several analytical functions are commonly used to describe the temporal profile of such a pulse, including Gaussian, Lorentzian, squared hyperbolic secant, exponential, and cardinal sine functions, etc.

The Gaussian function is the most widely used model for describing ultrashort pulses and is mathematically expressed as follows:

$$f(t) = e^{-\left(t/t_0\right)^2/2} = e^{-4\ln(2)\,t^2/\tau_p{}^2} \tag{1.49}$$

Using this formula (1.49), we have plotted in Figure 1.16 by python code the femtosecond Gaussian Pulse

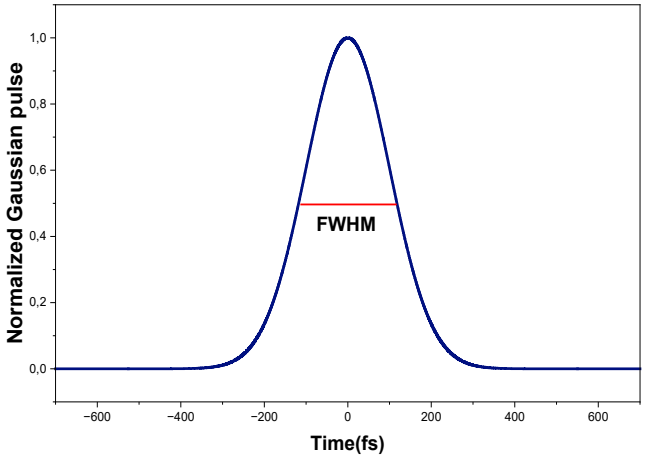

Figure 1.16: Gaussian model of Femtosecond Pulse.

1.4 Conclusion

Gold nanoparticles shows that their nanoscale behavior, influenced by complex optical and thermal effects, can be effectively described using suitable theoretical models in which plasmonic phenomena play a central role in controlling light absorption and energy transfer. The use of pulsed and femtosecond lasers allows the investigation of ultrafast processes, providing insight into electron-lattice interactions. Additionally, these laser-nanoparticle interactions can lead to the formation of transient bubbles in the surrounding medium, which is important for applications such as photothermal therapy and nanoscale material processing.

References of Chapter 1

[1] T. Dinh, Z. Dobó, Á. B. Palotás, H. Kovács, 2025, "A review of gold nanoparticle synthesis: Transitioning from conventional techniques to plant-mediated green nanofabrication," *Materials Today Chemistry*, vol. 48, p. 103003. https://doi.org/10.1016/j.mtchem.2025.103003

[2] F. Chen, Y. Wang, J. Ma, G. Yang, 2014, "A biocompatible synthesis of gold nanoparticles by Tris (hydroxymethyl)aminomethane," *Nanoscale Research Letters*, vol. 9, p. 220. https://doi.org/10.1186/1556-276X-9-220

[3] D. Rioux, 2015, "Synthèse et modélisation des propriétés optiques de nanoparticules d'alliage or-argent et leur application en imagerie hyperspectrale," PhD thesis, École Polytechnique de Montréal. https://publications.polymtl.ca/1815/

[4] J. Turkevich, P. C. Stevenson, J. Hillier, 1951, "A study of the nucleation and growth processes in the synthesis of colloidal gold," *Discuss. Faraday Soc.*, vol. 11, pp. 55–75. https://doi.org/10.1039/DF9511100055

[5] G. Frens, 1973, "Controlled Nucleation for the Regulation of the Particle Size in Monodisperse Gold Suspensions," *Nature Physics Science*. https://doi.org/10.1038/physci241020a0

[6] A. E. F. Oliveira, A. C. Pereira, M. A. C. Resende, L. F. Ferreira, 2023, "Gold Nanoparticles: A Didactic Step-by-Step of the Synthesis Using the Turkevich Method, Mechanisms, and Characterizations," *Analytica*, vol. 4, no. 2, pp. 250–263. https://doi.org/10.3390/analytica4020020

[7] M. Bouloudenine and M. Bououdina, 2016, "Toxic Effects of Engineered Nanoparticles on Living Cells", https://doi.org/10.4018/978-1-4666-9811-6.ch002

[8] E. Kianfar, 2025, "Gold Nanoparticles in Photothermal Cancer Therapy: Current Trends and Outlook," *Trends in Sciences*. https://doi.org/10.48048/tis.2025.9433

[9] Siddiqi and Husen, 2017, "Recent advances in plant-mediated engineered gold nanoparticles and their application in biological system," *Journal of Trace Elements in Medicine and Biology*. https://doi.org/10.1016/j.jtemb.2016.11.012

[10] M. Nour Mahamoud, 2025, "Elaboration de coques de nanoparticules d'or par voie émulsion: vers des nanorésonateurs plasmoniques," PhD thesis, Université de Rennes. https://theses.hal.science/tel-05483513

[11] T. Mitsudome, K. Kaneda, 2013, "Gold nanoparticle catalysts for selective hydrogenations," *Green Chemistry*. https://doi.org/10.1039/C3GC41360H

[12] J. Im et al., 2022, "Functionalized Gold Nanoparticles with a Cohesion Enhancer for Robust Flexible Electrodes," *ACS Applied Nano Materials*, vol. 5, no. 5, pp. 6708–6716. https://doi.org/10.1021/acsanm.2c00742

[13] H. Atwater, A. Polman, 2010, "Plasmonics for Improved Photovoltaic Devices," *Nature Materials*, vol. 9, p. 865. https://doi.org/10.1038/nmat2866

[14] I. Hammami, N. M. Alabdallah, A. A. Jomaa, M. Kamoun, 2021, "Gold nanoparticles: Synthesis properties and applications," *Journal of King Saud University – Science*. https://doi.org/10.1016/j.jksus.2021.101560

[15] A. R. Senoudi, 2010, "Étude des propriétés optiques des nanostructures métal composite par la méthode des éléments finis," doctorat thesis University of Tlemcen.

[16] K. L. Kelly, E. Coronado, L. L. Zhao, G. C. Schatz, 2002, "The Optical Properties of Metal Nanoparticles: The Influence of Size, Shape, and Dielectric Environment", https://doi.org/10.1021/jp026731y

[17] J. B. Vines et al., 2019, "Gold Nanoparticles for Photothermal Cancer Therapy," *Frontiers in Chemistry*, vol. 7. https://doi.org/10.3389/fchem.2019.00167

[18] S. Link, M. A. El-Sayed, 1999, "Spectral Properties and Relaxation Dynamics of Surface Plasmon Electronic Oscillations in Gold and Silver Nanodots and Nanorods", https://doi.org/10.1021/jp9917648

[19] A. Sitarski, 2017, "Development of Spectroscopic Methods for Dynamic Cellular Level Study of Biochemical Kinetics and Disease Progression".
[20] C. F. Bohren, D. R. Huffman, 1998, "Absorption and Scattering of Light by Small Particles," Wiley. https://doi.org/10.1002/9783527618156
[21] D. Manchon, 2012, "Réponse optique de nano-objets uniques anisotropes: de l'or aux métaux de transition", https://theses.fr/2012LYO10172
[22] A. Resano-Garcia, 2016, "Élaboration par ablation laser en milieu liquide de nanoparticules métalliques," PhD thesis, Université de Lorraine. https://theses.hal.science/tel-01544984
[23] E. D. Palik, 1998, "Handbook of Optical Constants of Solids," Academic Press.
[24] P. B. Johnson, R. W. Christy, 1972, "Optical Constants of the Noble Metals," *Physical Review B*, vol. 6, p. 4370. https://doi.org/10.1103/PhysRevB.6.4370
[25] A. E. R. Centeno, 2020, "Improved Drude-Lorentz dielectric function for gold nanospheres", https://doi.org/10.48550/arXiv.2012.05090
[26] A. Vial, T. Laroche, 2007, "Critical points model for dispersion properties of metals," *Journal of Physics D: Applied Physics*. https://doi.org/10.1088/0022-3727/40/22/043
[27] T. Bennour, 2018, "Modélisation des propriétés optiques de nanoparticules métalliques en milieu fluide : application à la conversion photo-thermique", Mémoire de Master, Université Mouloud Mammeri de Tizi-Ouzou.
[28] D. J. Griffiths, 2013, «Introduction of Electrodynamics », fourth edition, Pearson Education
[29] J.D. Jackson « Classical Electrodynamics » third edition 1999, JOHN WILEY & SONS, INC, p154,p158
[30] B. Palpant, 2012, "Photothermal Properties of Gold Nanoparticles", Gold Nanoparticles for Physics, Chemistry and Biology, pp. 75–102, https://doi.org/10.1142/9781848168077_0004
[31] G. V. Hartland, 2011, "Optical Studies of Dynamics in Noble Metal Nanostructures," *Chemical Reviews*. https://doi.org/10.1021/cr1002547
[32] M. G. Nicolas, M. M. Michel, and M. K.-C. Stéphane, 2018, "Master thesis related to nanocavitation and plasmonic nanoparticles", École Polytechnique de Montréal, https://publications.polymtl.ca/3261/1/2018_ViTchingdeLille.pdf
[33] A. Guglielmelli, F. Pierini, N. Tabiryan, C. Umeton, T. J. Bunning, L. De Sio, 2021, "Thermoplasmonics with Gold Nanoparticles: A New Weapon in Modern Optics and Biomedicine", https://doi.org/10.1002/adpr.202000198
[34] S. I. Anisimov, B. L. Kapeliovich, T. L. Perel'man, 1974, "Electron emission from metal surfaces exposed to ultrashort laser pulses", *Soviet Physics JETP*, vol. 39, pp. 375–377.
[35] J. Lombard, 2014, "Nanobulles et nanothermique aux interfaces", PhD thesis, Université Claude Bernard Lyon 1, https://tel.archives-ouvertes.fr/tel-01128228
[36] A. Dagallier, 2017, "Multiscale modeling of plasmonic enhanced energy transfer and cavitation around laser-excited nanoparticles", *Nanoscale*, 9, 3023–3032, https://doi.org/10.1039/C6NR08773F
[37] V. K. Pustovalov, 2005, "Theoretical Study of Heating of Spherical Nanoparticle in Media by Short Laser Pulses", https://doi.org/10.1016/j.chemphys.2004.08.005
[38] V. Pustovalov, Light-to-heat conversion and heating of single nanoparticles, their assemblies, and the surrounding medium under laser pulses Article in RSC Advances · August 2016 DOI: 10.1039/C6RA11130K
[39] "Laser Applications - an overview," ScienceDirect Topics. https://www.sciencedirect.com/topics/physics-and-astronomy/laser-applications
[40] S. K. Verma et al., 2012, "Laser in dentistry: An innovative tool," *National Journal of Maxillofacial Surgery*. https://doi.org/10.4103/0975-5950.111342
[41] K. Barat, 2002, "Laser Safety in Medicine," Springer. https://doi.org/10.1007/978-1-4615-0929-5_11
[42] M. H. Niemz, 2002, "Laser Dentistry," Springer. https://doi.org/10.1007/978-1-4615-0929-5_9
[43] "Laser Applications," Laser Scientist (website). https://laserscientist.com/laser-applications/

[44] R. Poprawe et al., 2004, "Laser Applications," Springer. https://doi.org/10.1007/b83824
[45] S. Affan Ahmed et al., 2021, "Survey and technological analysis of laser applications," *Defence Technology*. https://doi.org/10.1016/j.dt.2020.02.012
[46] F. Panthier et al., 2025, "Laser: Definition and technology," *French Journal of Urology*. https://doi.org/10.1016/j.fjurol.2025.102966
[47] R. Dabu, 2019, "Femtosecond Laser Pulses Amplification in Crystals," *Crystals*. https://doi.org/10.3390/cryst9070347
[48] J. A. Boyd, T. Lahaye, 2024, "A basic introduction to ultrastable optical cavities," *American Journal of Physics*. https://doi.org/10.1119/5.0161369
[49] "The Principles of Laser Generation," AlgoLaser (website). https://algolaser.com/blogs/how-to/the-principles-of-laser-generation
[50] B. N. Chichkov et al., 1996, "Femtosecond, picosecond and nanosecond laser ablation of solids," *Applied Physics A*. https://doi.org/10.1007/BF01567637
[51] Y. Qing, C. Guo, F. Chen and X. Hou, 2019, "A Review of Femtosecond Laser-Structured Superhydrophobic or Underwater Superoleophobic Porous Surfaces/Materials for Efficient Oil/Water Separation", https://doi.org/10.1039/C8RA10673H

Chapter two: Formation and Dynamics of Nanobubbles Around Gold Nanoparticles

2.1 Introduction

In the previous chapter, a general overview of gold nanoparticles and pulsed laser systems was presented. The main optical, thermal, and plasmonic properties of gold nanoparticles, as well as the fundamental characteristics of pulsed laser irradiation, were introduced. Having established these concepts, we now focus on the interaction between a pulsed laser and a gold nanoparticle immersed in a liquid medium (water).

This interaction can lead to a variety of thermal and mechanical phenomena, including nanoparticle heating, explosive boiling, and cavitation. Under appropriate irradiation conditions, these processes may result in the formation of vapor nanobubbles around the nanoparticle. The generation and dynamics of these nanobubbles play an important role in many applications, especially in medicine and cancer treatment.

In this chapter, we focus on several main aspects:

- We investigate the laser heating of gold nanoparticles and the subsequent heat transfer from the nanoparticles to the surrounding liquid medium.
- We discuss the possible transformations and physical phenomena that may occur during this thermal process.
- We examine the formation mechanisms of nanobubbles (nanocavitation).
- We study the dynamics of gold nanoparticles using the Rayleigh–Plesset equation, which is one of the most fundamental models used to describe bubble dynamics in a liquid. This equation governs the temporal evolution of a spherical bubble radius under the effects of pressure, surface tension, viscosity, and inertial forces, and is widely used to analyze cavitation and bubble growth–collapse behavior in fluid systems.

2.2 Laser–Plasmonic Nanoparticle Interaction in a Liquid

The interaction between the pulsed laser and plasmonic nanoparticles such as a gold nanoparticles can lead either to heating of the particle or to the formation of a nanoplasma depending on the laser parameters and the spectral detuning relative to the plasmonic resonance.

2.2.1 Heating the Nanoparticle

Heating a spherical metallic particle, such as a gold nanoparticle is generally achieved by laser irradiation at a wavelength close to its plasmonic resonance. This process relies on the coupling between the incident electromagnetic field of the laser and the collective oscillation

of the conductive elements of the nanoparticles. This phenomenon is known as localized surface plasmonic resonance [1] .

The process of heating gold nanoparticles occurs in three steps [2] :

- **Plasmon excitation and non-equilibrium electron generation:** Upon excitation of the localized surface Plasmon resonance (LSPR), the conduction electrons in the gold nanoparticle collectively oscillate under the electromagnetic field of the incident light. This collective oscillation leads to ultrafast absorption, leading to a non-equilibrium electronic state characterized by the formation of electron–hole pairs and highly excited electrons.
- **Electron–electron thermalization:** Electron–electron interactions rapidly redistribute the absorbed energy within the electron gas, causing a sharp increase in the electronic temperature T_e. This thermalization process occurs on an ultrafast timescale of a few femtoseconds.
- **Electron–phonon coupling:** The excited electrons subsequently transfer their energy to the nanoparticle lattice through electron–phonon coupling. As a result, the lattice temperature rises over a timescale of a few picoseconds, eventually leading to thermal equilibrium between the electrons and the lattice($T_e = T_L$).

2.2.2 Heat dissipation to the surrounding medium

There are two different ways to heat the surrounding water [3] :

1. The first mechanism involves the formation of a nanoplasma and takes place on an ultrafast timescale. At high laser fluences, the absorbed energy is rapidly transferred from the plasma to the surrounding water molecules within a few femtoseconds. Because this energy deposition occurs much faster than the characteristic hydrodynamic expansion time, the water experiences an almost isochoric heating process (constant volume).
2. The second mechanism is thermal conduction, which dominates at lower laser fluences. In this case, the absorbed energy is first transferred to the nanoparticle lattice and subsequently diffuses into the surrounding water over timescales of a few picoseconds. Compared with nanoplasma-mediated heating, this process is significantly slower and leads to a more gradual increase in the temperature of the liquid environment.

The ultrafast transfer of heat from the nanoparticle to the surrounding liquid produces a substantial localized temperature rise, followed by the cooling of the nanoparticle. Depending

on the heating conditions, the liquid may undergo different thermodynamic transformations and phase transitions, which can be interpreted using the phase diagram (see Figure 2.1).

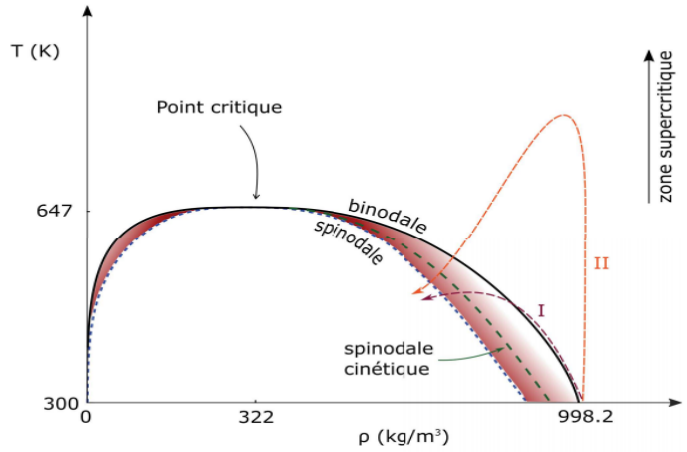

Figure 2.1: Temperature-Density phase diagram of water illustrating the critical point, binodal curve and spinodal boundary [4] .

The critical point: defines the conditions beyond which the liquid and vapor phases become indistinguishable. At this point, the distinction between the two phases disappears, and the fluid exists as a supercritical fluid [5] .

The binodal curve: represents the boundary at which the liquid and vapor phases coexist under thermodynamic equilibrium. Along this curve, the pressure, temperature, and chemical potential are identical in both phases.

The spinodal curve: represents the absolute stability limit of the metastable liquid state. At this boundary, the liquid loses its thermodynamic stability, and even infinitesimal fluctuations can trigger a spontaneous phase transition. Beyond the spinodal limit, the liquid becomes intrinsically unstable and rapidly transforms into vapor [4] . For water at atmospheric pressure, the spinodal temperature T_{spin} is approximately 550 K, corresponding to about 0,85 T_c to 0,9 T_c, where T_c is the critical temperature of water [6] .

The metastable region: is located between the binodal and spinodal curves. In this region, water remains in the liquid state despite being heated above its saturation temperature. Although the liquid is still stable, it is highly sensitive to perturbations, which can initiate bubble nucleation and lead to a phase transition.

Following the introduction of the phase diagram, various phenomena related to the liquid-to-vapor transition can be analyzed, such as normal evaporation, explosive evaporation, and cavitation.

1. The normal boiling of water

Normal boiling of water is the phase change from liquid to vapor (vaporization) that occurs under thermodynamic equilibrium conditions and it follows the binodal curve (see Figure 2.1), which defines the saturation limit in the phase diagram. This process takes place when the water reaches its boiling temperature, $T_{boild} = 373\,\mathrm{K}$ in the curve at the atmospheric pressure $P_{atm} \approx 10^5\mathrm{Pa}$.

2. Explosive boiling

Explosive boiling, also known as explosive phase transition, is a rapid liquid-to-vapor phase change that occurs when the liquid is heated above its local boiling point under near-constant pressure conditions. It typically arises when the liquid is subjected to extremely high temperatures over very short timescales [7].

Unlike normal boiling, explosive boiling occurs out of equilibrium occurs near the spinodal limit, which is the stability limit in the phase diagram (see Figure 2.1), and it occurs when reaches the spinodal temperature $T_{spin} = 0.9 \times T_c$, where T_c is the critical temperature of water.

3. Cavitation

Cavitation is the formation and activity of bubbles or cavities [8] , and it is defined as the nucleation process of vapor bubbles in a liquid. It occurs through a decrease in pressure at an approximately constant temperature [9] .

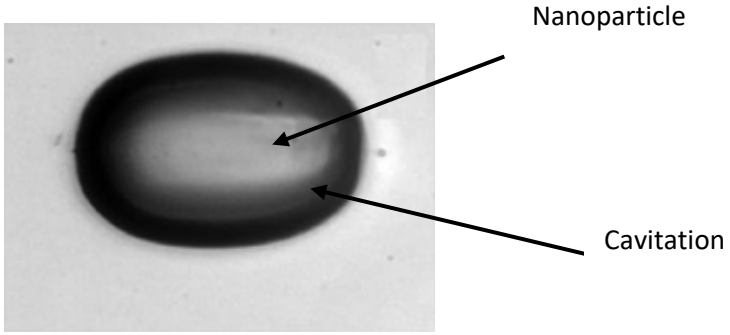

Figure 2.2: Laser-Induced Cavitation around a Gold Nanoparticle [10] .

a. Classification of Cavitation Phenomena

The phenomenon of cavitation can be classified according to its underlying physical mechanisms into two main categories (see Table 2.1).

Table 2.1: represents the two categories of the Cavitation Phenomena [8] .

Cavitation Induced by Liquid Tension		***Cavitation Induced by Local Energy Deposition***	
Hydrodynamic Cavitation	***Acoustic Cavitation***	***Optical Cavitation***	***Particle Cavitation***
Resulting from pressure variations related to the flow of the liquid.	Induced by a pressure field, usually an acoustic wave.	Initiated by high-intensity laser pulses that induce local breakdown of the liquid, leading to bubble formation.	This phenomenon is based on the growth of bubbles in a superheated liquid through which a charged particle passes.

b. Cavitation threshold:

The liquid phase, such as water, plays a fundamental role in the study of phase transitions and phenomena such as cavitation and vaporization.

A liquid can flow like a fluid but it can also resist tensile stresses (negative pressure). It is a breaking stress or the maximum negative pressure that a liquid can withstand before its structure breaks down to form a cavity (bubble).

Figure 2.3: Tensile Stress (Negative Pressure) in Liquids.

c. Cavitation Nucleation:

Nucleation is the fundamental process of vapor bubble formation in a liquid; it occurs when a decrease in pressure causes the liquid's structure to rupture [11]. This can occur in two main categories [12] :

- **Homogeneous nucleation:** occurs in a perfectly pure liquid, where random thermal motion of molecules leads to the formation of temporary microscopic voids that can act as nuclei for bubble formation and rupture.
- **Heterogeneous nucleation**: This occurs at surfaces such as the container walls or on particles suspended in the liquid. The presence of impurities significantly reduces the rupture stress required for bubble formation, thus greatly facilitating the initiation of cavitation.

Cavitation usually begins from pre-existing sites known as 'nuclei'. These nuclei typically take the form of micro-bubbles extremely small gas bubbles, which are either dispersed in the liquid or trapped in surface [11] .

2.3 The Formation of Nanobubbles around heated nanoparticles

For plasmonic nanoparticles irradiated by ultrashort-pulsed lasers, phase transition and nanobubble formation result from a combination of two mechanisms: thermally driven phase explosion and mechanically induced cavitation. The following table provides a comparative summary of these two phenomena [4] .

2.3.1 Formation mechanism

The formation mechanisms in laser-irradiated gold nanoparticles under pulsed laser excitation are complex and depend on several nanoparticle and laser parameters, including in particular the nanoparticle diameter, thickness, and shape, as well as the laser fluence and pulse duration.

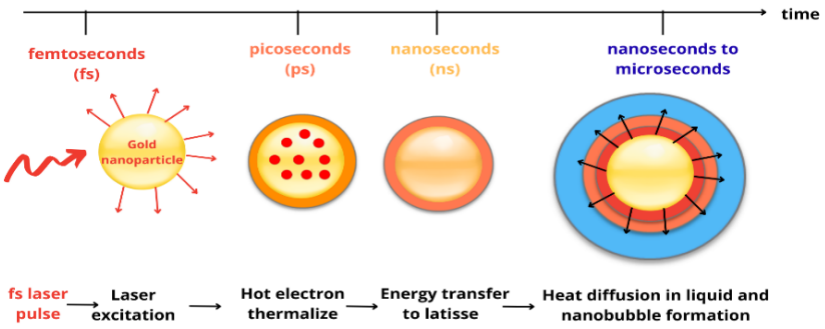

Figure 2.4: Mechanism of Gold Nanoparticle Heating, Heat Transfer and Nanobubble formation.

When a laser pulse irradiates a gold nanoparticle, the absorbed energy is initially deposited into its free electrons, resulting in a rapid increase in the electron temperature. This thermal energy is subsequently transferred to the nanoparticle lattice and then to the surrounding liquid, depending on the irradiation conditions.

Rapid heating of a liquid can trigger various phase-change mechanisms. Depending on the temperature reached and the thermodynamic conditions of the system, the following 2 cases may occur:

- ***Case 1:*** If the maximum temperature reached along the binodal curve remains below the nucleation threshold, typically in the range of $T_{nuc} \approx 0{,}9\ T_c$, no bubble formation occurs.
- ***Case 2:*** During ultrafast heating, water cannot follow the normal equilibrium boiling pathway along the binodal curve. Consequently, the liquid temperature increases beyond the binodal boundary and penetrates the metastable region of the phase diagram (see Figure 2.1).
  - When the temperature reaches the spinodal limit, estimated at approximately 550 K ($\sim 0{,}85 - 0{,}9\ T_c$, with T_c= 647 K), water undergoes a rapid and violent liquid-to-vapor phase transition. This process is referred to as phase explosion, which may result in various physical effects:
    - ✓ **Shock wave (pressure):** phase explosion generates an intense pressure wave that propagates into the surrounding liquid at a velocity close to the speed of sound.
    - ✓ **Nanobubble formation:** this pressure wave can generate negative pressure (tensile stress), leading to cavitation and the formation of vapor cavities (nanobubbles).

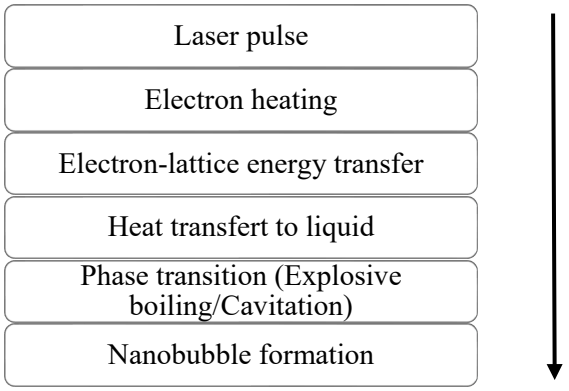

Figure 2.5: Schematic Representation of Laser-Induced Nanobubble Formation.

Important Remarks :

- A number of factors, including the geometry of the gold nanoparticle, the nature of the surrounding liquid, the laser fluence, and the pulse duration, governs the formation of nanobubbles. Variations in these parameters can significantly affect the onset of cavitation and the subsequent dynamics of bubble formation.
- The formation of a nanobubble requires the attainment of critical threshold conditions of water in terms of temperature, pressure, volume and density. These thresholds can be determined using thermodynamic models such as the Van der Waals equation:

Critical temperature: $T_c = \frac{8a}{27\,Rb}$

Critical pressure: $P_c = \frac{a}{27\,b^2}$

Critical volume: $V_c = 3b$

Critical density: $\rho_c = \frac{M}{V_c}$

Where a and b are constants of Van der Waals, R is the constant of ideal gas and M is the molar mass of water.

Beyond their fundamental physical interest, laser-induced nanobubbles have attracted considerable attention due to their potential applications in biomedical imaging, drug delivery and photothermal therapies.

Nanobubbles in the biomedical field are considered part of theranostic techniques that combine imaging, diagnosis, and therapy, especially for early cancer treatment. They are formed when nanoparticles absorb laser light and convert it into heat, generating localized mechanical effects on target cells. They also improve medical imaging by light scattering and reduce damage to healthy cells, making treatment more precise and selective [13].

2.4 Nanobubble Dynamics

The life cycle of the nanobubble generated around a laser-heated nanoparticle can be divided into three distinct stages: nucleation, growth, and collapse (see Figure 2.6).

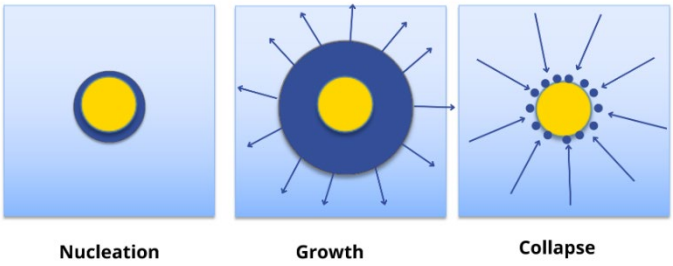

Figure 2.6: Nucleation, Growth and Collapse of a Nanobubble.

Following the nucleation of a vapor nanobubble (or nanocavitation), the bubble nucleus undergoes rapid expansion. Because this process takes place over an extremely short timescale, heat transfer is predominantly ballistic rather than diffusive [14]. The nanobubble then continues to grow until it reaches a temporary equilibrium state, where the external pressure, surface tension effects, and viscous forces balance the internal vapor pressure. At this stage, the bubble attains its maximum radius and a transient state of mechanical equilibrium.

After reaching its maximum radius, the bubble begins to collapse under the combined action of the surrounding liquid pressure and surface tension. In general, bubble expansion is significantly faster than its collapse.

2.4.1 Rayleigh-Plesset equation

The dynamics of a spherical bubble radius can be described by the Rayleigh–Plesset equation, which is introduced by Lord Rayleigh (1917) and later extended by Plesset [13] . This model allows the study of bubble dynamics under the influence of pressure, surface tension, and viscous effects.

We consider a bubble of radius $R(t)$ in a homogeneous liquid of constant density ρ_L and pressure P_∞ far from the bubble.

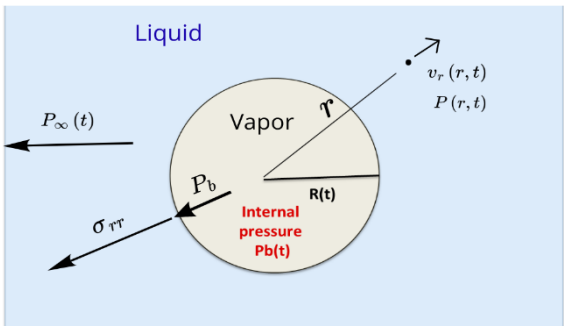

Figure 2.7: Schematic representation of spherical vapor bubble in liquid and the forces governing its dynamics.

The radial velocity of the liquid $\vec{v}(r,t)$ at a distance r from the center of the bubble is governed by the continuity equation. If we assume that, the liquid is incompressible:

$$\nabla.\vec{v} = 0 \tag{2.1}$$

In spherical coordinates (r,θ,ϕ) :

$$\frac{1}{r^2}\frac{\partial}{\partial r}(r^2 v_r) + \frac{1}{r\sin\theta}\frac{\partial}{\partial\theta}(v_\theta \sin\theta) + \frac{1}{r\sin\theta}\frac{\partial v_\phi}{\partial\phi} = 0 \tag{2.2}$$

with spherical symmetry, the components of the velocity v along the angles θ and ϕ are zero, so we can write:

$$\nabla.\vec{v} = \frac{1}{r^2}\frac{\partial}{\partial r}(r^2 v_r) = 0 \tag{2.3}$$

Integrating equation (2.3), we find:

$$r^2 v_r = f(t) \tag{2.4}$$

$$\Rightarrow v_r(r,t) = \frac{f(t)}{r^2} \tag{2.5}$$

where $f(t)$ is related to *R*(*t*) by a kinematic boundary condition at the bubble surface [11].

If mass transport at the bubble interface is neglected where $r = R$, the liquid velocity is equal to the wall velocity:

$$v_r(R,t) = \frac{dR}{dt} = \frac{f(t)}{R^2} \tag{2.6}$$

$$\Rightarrow f(t) = R^2\frac{dR}{dt} \tag{2.7}$$

$$\Rightarrow v_r(r,t) = \frac{R^2.\dot{R}}{r^2} \tag{2.8}$$

The movement of the liquid is governed by the Navier-Stokes equation in polar coordinates for the radial direction:

$$-\frac{1}{\rho_L}\frac{\partial p}{\partial r} = \frac{\partial v_r(r,t)}{\partial t} + v_r(r,t)\frac{\partial v_r(r,t)}{\partial r} - \nu_L\left[\frac{1}{r^2}\frac{\partial}{\partial r}(r^2 v_r) - \frac{2v_r(r,t)}{r^2}\right] \tag{2.9}$$

For high Reynolds number flows, viscous diffusion inside the bulk is neglected ($\nu_L = 0$), yielding:

$$-\frac{1}{\rho_L}\frac{\partial p}{\partial r} = \frac{\partial v_r(r,t)}{\partial t} + v_r(r,t)\frac{\partial v_r(r,t)}{\partial r} \tag{2.10}$$

Substituting Equation (2.8) into Equation (2.10), gives:

$$-\frac{1}{\rho_L}\frac{\partial p}{\partial r}=\frac{\partial}{\partial t}\left(\frac{R^2.\dot{R}}{r^2}\right)+\frac{R^2.\dot{R}}{r^2}\frac{\partial}{\partial r}\left(\frac{R^2.\dot{R}}{r^2}\right) \tag{2.11}$$

After differentiation and simplification:

$$-\frac{1}{\rho_L}\frac{\partial p}{\partial r}=\frac{2\,R^2\dot{R}+R^2\ddot{R}}{r^2}-\frac{2\,R^4\dot{R}^2}{r^5} \tag{2.12}$$

Integrating Equation (2.12) from r to ∞ where P to P_∞, gives:

$$\frac{1}{r}\left(2\,R^2\dot{R}+R^2\ddot{R}\right)-\frac{1}{4r^4}\left(2\,R^4\dot{R}^2\right)=\frac{P(R,t)-P_\infty}{\rho_L} \tag{2.13}$$

Equation (2.13) is simplified by setting (r = R) at the bubble surface:

$$R\ddot{R}+\frac{3}{2}\dot{R}^2=\frac{P(R,t)-P_\infty}{\rho_L} \tag{2.14}$$

The normal stress in the liquid at the interface:

$$\sigma_{rr}(R)=-P(R,t)+2\mu_L\left.\frac{\partial v_r}{\partial r}\right|_{r=R} \tag{2.15}$$

From Equation (2.8):

$$\left.\frac{\partial v_r}{\partial r}\right|_{r=R}=-\frac{2\dot{R}}{R} \tag{2.16}$$

Thus:

$$\sigma_{rr}(R)=-P(R,t)-\frac{2\mu_L\dot{R}}{R} \tag{2.17}$$

The stress balance at the bubble interface is:

$$\sigma_{rr}(R)+P_b-\frac{2S}{R}=0 \tag{2.18}$$

Substituting Equation (2.17) into Equation (2.18), gives:

$$-P(R,t)-\frac{2\mu_L\dot{R}}{R}+P_b-\frac{2S}{R}=0 \tag{2.19}$$

$$\Rightarrow P(R,t)=P_b-\frac{2S}{R}-\frac{2\mu_L\dot{R}}{R} \tag{2.20}$$

Substituting Eq. (2.20) into Eq. (2.14), the classical Rayleigh–Plesset equation is obtained:

$$\frac{1}{\rho_L}\left(R\ddot{R}+\frac{3}{2}\dot{R}^2\right)=(P_b-P_\infty)-\frac{2S}{R}-\frac{2\mu_L\dot{R}}{R} \tag{2.21}$$

- $R(t)$: The radius of the bubble
- $\dot{R}(t)$: The velocity of bubble.
- $\ddot{R}(t)$: The acceleration of bubble.
- P_b: The pressure inside the bubble.
- P_∞ : The ambient pressure.
- μ_L: The dynamic viscosity.
- S: The surface tension.

The Rayleigh–Plesset equation is a second-order ordinary differential equation (ODE) in time. We can apply a transformation to reduce the second-order Rayleigh–Plesset equation (2.21) to a first-order linear differential equation. If we put:

$$V=\frac{dR}{dt}=\dot{R} \quad \text{and} \quad \frac{dV}{dt}=\ddot{R} \tag{2.22}$$

The Equation (2.21) becomes:

$$\frac{1}{\rho_L}\left(R\frac{dV}{dt}+\frac{3}{2}V^2\right)=(P_b-P_\infty)-\frac{2S}{R}-\frac{2\mu_L V}{R} \tag{2.23}$$

In the literature, two formulations of the Rayleigh–Plesset equation are found: either the complete form or a simplified form. To simplify the Rayleigh-Plesset equation, we neglect the dynamic viscosity and the tension surface, the Equation (2.23) becomes:

$$\frac{1}{\rho_L}\left(R\frac{dV}{dt}+\frac{3}{2}V^2\right)=P_b-P_\infty \tag{2.24}$$

The pressure inside the bubble can be modeled as:

$$P_b=P_v \tag{2.25}$$

where P_v is the vapor pressure.

For laser-induced cavitation around gold nanoparticles, the Clausius-Clapeyron model is one of the models who commonly used to relate the vapor pressure inside the bubble to its temperature:

$$P_b=P_v(T)=P_{ref}\exp\left(-\frac{\Delta H_v}{R_{gas}}\left(\frac{1}{T}-\frac{1}{T_{ref}}\right)\right) \tag{2.26}$$

where P_{ref} the reference vapor pressure (Pa), T_{ref} is the reference temperature (K), R_{gas} is the universal gas constant (8,314 $\text{Jmol}^{-1}\text{K}^{-1}$) and ΔH_v is the molar enthalpy of vaporization of water (Jmol^{-1}). Typically, T_{ref} =373 K, P_{ref} =1 atm.

Substituting Eq. (2.26) into Eq. (2.24), we obtain:

$$\frac{1}{\rho_L}\left(R\frac{dV}{dt}+\frac{3}{2}V^2\right)=P_{ref}\ exp\left(-\frac{\Delta H_v}{R_{gas}}\left(\frac{1}{T}-\frac{1}{T_{ref}}\right)\right)-P_{\infty} \tag{2.27}$$

In the Clausius–Clapeyron equation, T is taken as T_s, the Au/water interfacial temperature delivered by the TTM, which resolves the electron temperature T_e, the lattice temperature T_L, and the interface temperature T_s as it is this latter quantity that directly drives the liquid-to-vapor phase transition.

Several models can be used to estimate the internal pressure of a bubble, such as the van der Waals model and other thermodynamic approaches. There are other models, depending on the assumptions and modeling conditions [13].

References of Chapter 2:

[1] Novotny, L., & Hecht, B. (2012). Principles of Nano-Optics (2e éd.). Cambridge University Press.

[2] Nicolas, M. G., Michel, M. M., & Stéphane, M. K.-C. (2018). Caractérisation de la nanocavitation de nanoparticules plasmoniques irradiées hors-résonance par impulsions ultra-brèves [Thèse de doctorat, Polytechnique Montréal].

[3] Boulais, E. (2013). Modélisation de l'interaction entre une impulsion laser ultrabrève et une nanostructure plasmonique en milieu aqueux [Thèse de doctorat, École Polytechnique de Montréal].

[4] Dagallier, A. (2021). Dynamique de nanobulles et nanoplasmas générés autour de nanoparticules plasmoniques irradiées par des impulsions ultracourtes [Thèse de doctorat, Polytechnique Montréal].

[5] ThoughtCo. (2026). What Does Critical Point or Critical State Mean? Consulté le 7 juin 2026. Disponible sur : https://www.thoughtco.com/definition-of-critical-point-605853

[6] Maheshwari, S., Van Der Hoef, M., Prosperetti, A., & Lohse, D. (2018). Dynamics of formation of a vapor nanobubble around a heated nanoparticle. Journal of Physical Chemistry C, 122(36), 20571–20580. https://doi.org/10.1021/acs.jpcc.8b04017

[7] Xu, X., Chen, G., & Song, K. H. (1999). Experimental and numerical investigation of heat transfer and phase change phenomena during excimer laser interaction with nickel. International Journal of Heat and Mass Transfer, 42(8), 1371–1382. https://doi.org/10.1016/S0017-9310(98)00272-5

[8] Young, F. R. (1999). Cavitation. World Scientific Publishing.

[9] René, P. (2015). La cavitation : une introduction [Note de cours, École Nationale Supérieure d'Arts et Métiers].

[10] Bhuyan, M., Soleilhac, M., Somayaji, M., Itina, T., Antoine, R., & Stoian, R. (2018). High fidelity visualization of multiscale dynamics of laser-induced bubbles in liquids containing gold nanoparticles. Scientific Reports, 8, Article 9283. https://doi.org/10.1038/s41598-018-27663-z

[11] Brennen, C. E. (2023). Cavitation and Bubble Dynamics (The Oxford Engineering Science Series, No. 44). Oxford University Press. https://doi.org/10.1093/oso/9780195094091.001.0001

[12] Elsevier. (2025). Nucleation of single acoustic cavitation bubble: modeling and simulation. Dans Modeling and Simulation of Sono-Processes (pp. 71–90). Elsevier. https://doi.org/10.1016/B978-0-443-23651-8.00005-X

[13] Lombard, J. (2016). Nanobulles et nanothermique aux interfaces [Thèse de doctorat, Université Claude Bernard Lyon 1].

[14] Lombard, J., Biben, T., & Merabia, S. (2015). Nanobubbles around plasmonic nanoparticles: Thermodynamic analysis. Physical Review E, 91(4), Article 043007. https://doi.org/10.1103/PhysRevE.91.043007

Chapter 3: Simulation of Nanocavitation and Results

3.1 Introduction

In this chapter, we present and analyze the results obtained from the numerical model developed to study the generation and dynamics of a vapor nanobubble around a gold nanoparticle irradiated by a femtosecond laser. Calculating the evolution of the nanobubble radius using the Rayleigh-Plesset equation requires the prior determination of several physical quantities. The different calculation steps are as follows:

- Calculation of the absorption cross-section of the gold nanoparticle.
- Determination of the electronic and lattice temperatures using the Two Temperature Model (TTM).
- Calculation of the temperature at the nanoparticle-water interface, taking into account the heat transfer between the nanoparticle and the liquid medium.
- Determination of the nanobubble nucleation conditions from the interfacial temperature.
- Solving the Rayleigh-Plesset equation to study the growth dynamics of the nanobubble.

Since the TTM and the Rayleigh–Plesset equation both reduce to first-order ordinary differential systems, their numerical integration was carried out using the *scipy.integrate.solve_ivp* routine, introduced in Python 3.13, with the RK45 solver (adaptive scheme), which provides automatic step-size control and high numerical accuracy.

3.2 Calculation of the absorption cross sections σ_{abs}

The calculation of the absorption cross-section σ_{abs} is performed by returning equations (1.35, 1.36 and 1.37) in Chapter 1, using the Drude-Lorenz model, which was calculated in Chapter 1 using equation (1.21). We present the Python code that was used to model the absorption cross section and the corresponding plots can be found in Figure 3.1.

Code Python: Optical cross Section

```
eps_m=1.77
n_m=1.33
 # Nanoparticle radius (nm)
R=30
# Volume
V=(4/3)*np.pi* R**3
 # Total dielectric function
    epsilon = eps_drude + eps_lorentz
    epsilon1[i] = epsilon.real
    epsilon2[i] = epsilon.imag
    # Polarizability
    alpha=3*V*((epsilon - eps_m)/(epsilon + 2*eps_m))
    # Wave vector
    k=2*np.pi*n_m/lam
    # Cross sections
    sigma_abs[i]=k*np.imag(alpha)
    #sigma_sca[i]=((k**4)/(6*np.pi))*np.abs(alpha)**2
    sigma_sca[i]=((k**4)/(6*np.pi))*(alpha.real**2+alpha.imag**2)
    sigma_ext[i]=(sigma_abs[i] + sigma_sca[i])
# Maximum absorption
max_abs = np.max(sigma_abs)
print("Maximum absorption =", max_abs)
# Save data
file = open("section.dat", "w")
for i in range(N):
    file.write("{:10.2f} {:15.6f} {:15.6f} {:15.6f}\n".format(lambda_[i], sigma_ext[i],
sigma_sca[i], sigma_abs[i]))
file.close()
# Plot
plt.plot(lambda_,sigma_ext,label="Extinction")
plt.plot(lambda_,sigma_sca,label="Scattering")
plt.plot(lambda_,sigma_abs,label="Absorption")
plt.xlabel("Wavelength (nm)")
plt.ylabel("Cross sections")
plt.title("Optical Cross Sections of Gold Nanoparticles")
plt.legend()
```

Note: The first part of the code was implemented in Chapter 1 using the Drude-Lorentz model on page 5.

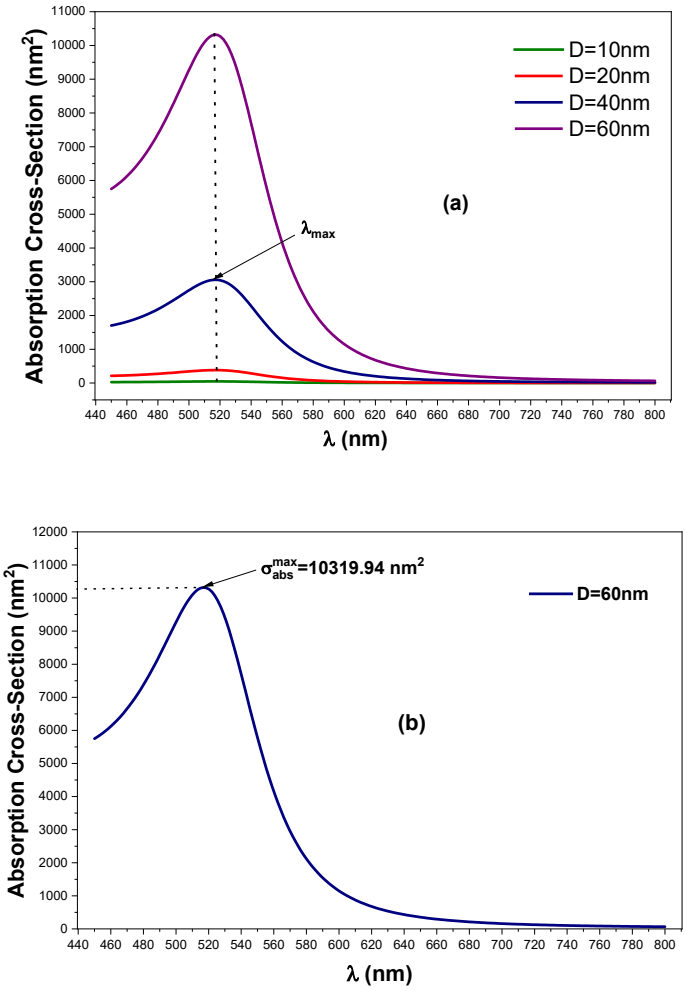

Figure 3.1: Absorption cross- sections of a gold nanoparticle of different diameters D=2a in the water with permittivity ε_m = 1.77 (a). Absorption cross sections of a gold nanosphere of diameters D=60nm in the water (b).

In Figure 3.1 (a): we have plotted the absorption cross sections as a function of wavelength for different diameters in the water:

- Nanoparticle presents a maximum absorption which appears around $\lambda \approx 520\, nm$, corresponding to the localized surface plasmon resonance (LSPR).
- Curve (a) shows the effect of diameter on the absorption of a gold nanoparticle. We observed that the absorption cross section increases as the nanoparticle diameter increases.

In Figure 3.1 (b): We have plotted the absorption cross sections as a function of wavelength for diameter D=2a=60 nm and it is found that for the maximum wavelength $\lambda_{max} \approx 520\, nm$, the absorption cross-section $\sigma_{abs}^{max} = 10319{,}94\, nm^2$ (data used in the next simulation).

3.3 Calculation of The Two-Temperature models TTM

After calculating the absorption cross-section, we calculate the power contained in the TTM [1] using the formula:

$$S(t) = \frac{F_P}{\tau_P}\frac{\sigma_{abs}}{V_P}\, f(t)$$

where $f(t)$ the Gaussian profile of the laser pulse [1] :

$$f(t) = e^{-4\ln(2)\,(t-2\tau_P)^2 / \tau_p{}^2}$$

Then we calculate the electronic temperature T_e and the lattice temperature T_L which represent the ultrafast thermal dynamic, introduced through the TTM model in Chapter 1 using equations (1.35, 1.36 and 1.41).

Table 3.1: The Parameters used in TTM Simulation.

	Physical parameters	**Value**
Gold Nanoparticle	Nanoparticle radius a (nm)	30
	Density ρ_{gold} (Kg m^{-3})	$1{,}93 \times 10^4$ [2]
	Volume of the gold nanoparticle V_P (m^3)	$4 \times \pi \times a^3/3$
	Surface of the gold nanoparticle S_P (m^2)	$4 \times \pi \times a^2$
	Electron-phonon coupling factor g (Wm^{-3} K^{-1})	$2{,}2 \times 10^6$ [5]
	Electron heat capacity C_e (Jm^{-3} K^{-1})	$C_e = 70 \times T_e$ [2]
	Lattice heat capacity C_L (Jm^{-3} K^{-1})	$C_L = \rho_{gold} \times (109{,}707\, T_L - 3{,}4 \times 10^{-4}\, {T_L}^2 + 5{,}24 \times 10^{-7} {T_L}^3 - 3{,}93 \times 10^{-10} {T_L}^4 + 1.17 \times 10^{-13} {T_L}^5)$ [3]
	The absorption cross-section σ_{abs}^{max} (nm^2) Computed by Python code chapter 3, p47	10319,94
Laser	Laser fluence F_P (Jm^{-2})	5
	Pulse width τ_P	$\tau_P = 200$ fs and $\tau_P = 100$ ps
Water	The ambient water temperature T_∞ (K)	300
	The thermal conductivity of water k_∞ at T_∞ (W/K/m)	0,61 [4]
	Thermal conductance at the (Au/water) interface G (Wm^{-2} K^{-1})	105×10^6 [4]

The coding section will be provided in the section on calculating the dynamics of Nano cavitation, and we have plotted in Figure 3.2 the variation of electronic temperature T_e and lattice temperature T_L as a function of time (t) for a femtosecond laser $\tau_P = 200$ fs and picosecond laser $\tau_P = 100$ ps.

Both the electron and lattice temperatures are initialized to room temperature, i.e., $T_e = T_L = 300\ K$.

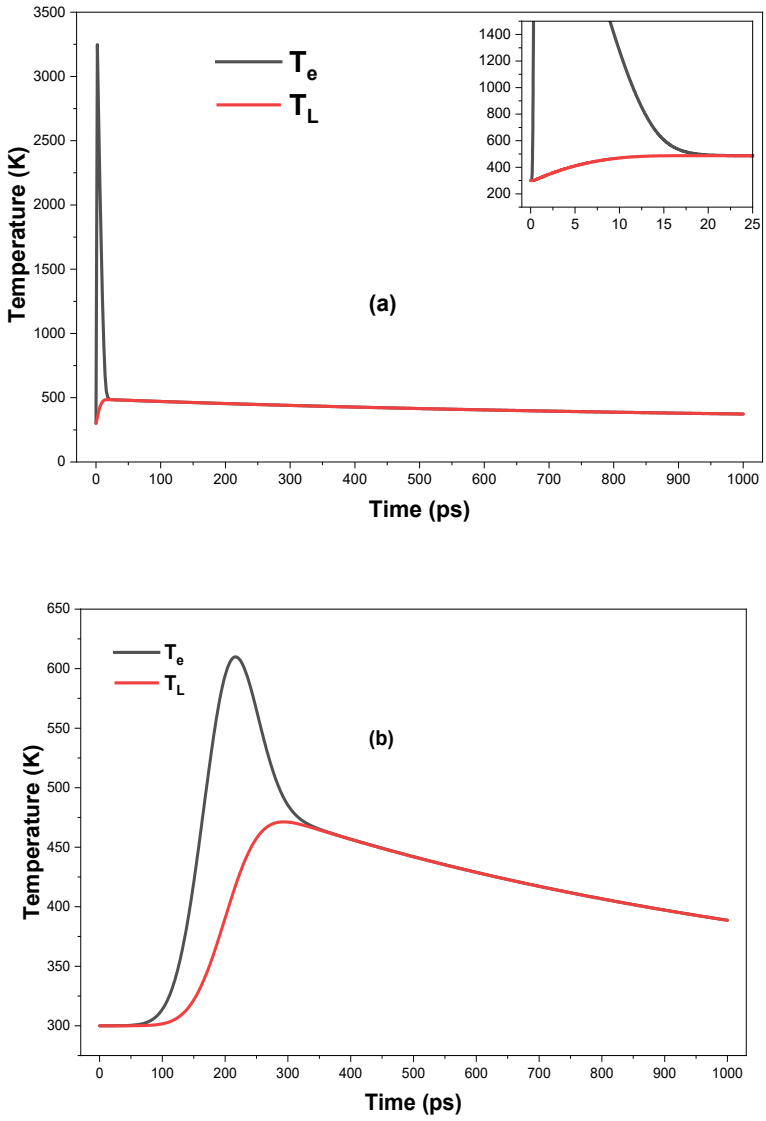

Figure 3.2: Evolution of electronic temperature T_e and lattice temperature T_L as a function of time (ps) with $D = 2a = 60nm$,(a) $\tau_P = 200$ fs; (b) $\tau_P = 100$ ps.

Figure 3.2 shows the ultrafast thermal dynamics, which occurs in picoseconds within the gold nanoparticles under picosecond and femtosecond pulse duration.

In the Figure 3.2 (a): the variation of T_e and T_L as a function of time (t) for a pulse duration $\tau_P = 200$ fs .

- The electronic temperature T_e increases very rapidly, reaching a value of approximately 3250 K due to rapid absorption by electrons.

- The lattice temperature T_L increases more slowly than T_e until it reaches a value of approximately 500 K because the energy transfer of electrons to the lattice requires a certain amount of time.
- Both temperatures T_e and T_L start to decrease and eventually converge to the same value at a time ranging fro 16 ps to 20 ps this is the state of thermal equilibrium where (T_e =T_L).
- This decrease is due to heat transfer to the external environment (water).

In the Figure 3.2 (b): the variation of T_e and T_L as a function of time (t) for a pulse duration $\tau_P = 100$ ps .

- This figure shows the effect of laser pulse duration.
- We observe the same general behavior as in Figure 3.2 (a), but because of the pulse duration $\tau_P = 100$ ps, the T_e reaches a maximum value of approximately 620 K, lower compared to the case of $\tau_P = 200$ fs. This means that the heating of the electrons is more gradual in the picosecond regime.
- Both temperatures T_e and T_L start to decrease and eventually converge to the same value at a time ranging from 300 ps to 350 ps this is the state of thermal equilibrium where (T_e = T_L).

3.4 The temperature of the Au/water interface T_s

The Au/water interface temperature T_s is the temperature of the medium at the point of contact with the surface of the gold nanoparticle [5], which is written in the form:

$$Q = GS_P\,(T_L(t) - T_s(t)) \;\rightarrow\; T_s(t) = T_L(t) - \frac{Q}{GS_P}$$

where G is the interface thermal conductivity and S_P is the surface of the spherical AuNP.

The calculation of this temperature is done using Python code and it will be given later in the overall program in the section on calculating the dynamics of nanocavitation, and we have plotted in figure 3.3 the variation of The Au/water interface temperature T_s as a function of time (t) for a femtosecond laser $\tau_P = 200$ fs and picosecond laser $\tau_P = 100$ ps .

In the Figure 3.3: The evolution of the Au/water interface temperature T_s as a function of time with $D = 2a = 60$nm for $\tau_P = 200$ fs and $\tau_P = 100$ ps, we can observe:

- That in the both cases, the temperature exceeds the boiling point of water.
- For the femtosecond pulse $\tau_P = 200$ fs , the temperature remains close to ambient temperature at the beginning, then increases rapidly to reach a maximum of about 430K around 280 ps to 300 ps.
- For the picosecond pulse $\tau_P = 100$ ps, the temperature increases much earlier and then quickly reaches a maximum close to 440 K within the first few picoseconds.

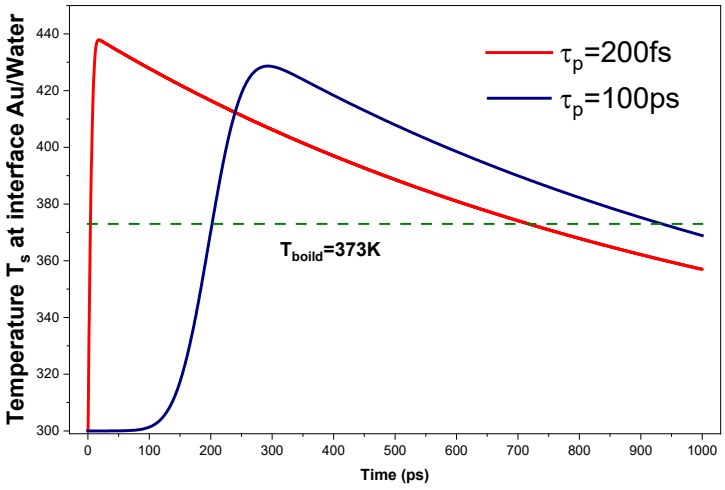

Figure 3.3: Evolution of the Au/water interface temperature T_s as a function of time (t) with $D = 2a = 60\text{nm}$ for time duration $\tau_P = 200$ fs and $\tau_P = 100$ ps.

3.5 The Rayleigh-Plesset Equation

After calculating the absorption cross-section and analyzing the temperature evolution using the Two-Temperature Model (TTM), as well as the temperature of interface T_s, we now solve the Rayleigh-Plesset equation (Eq.2.21, Chapter 2) for investigate the dynamics of the nanobubble generated around the gold nanoparticle.

Table 3.2: The Physical Parameters used in Rayleigh-Plesset Simulation.

Material parameters	**Value**
Initial value of nanobuble R0 (nm)	30
The dynamic viscosity of water μ_L (m^3)	10^{-3}
The surface tension of water S (m^2)	0,072
Density of water ρ_L $(\text{Wm}^{-3}\ \text{K}^{-1})$	1000
The absorption cross-section σ_{abs}^{max} (nm^2)	10319,94
Laser fluence F_P (Jm^{-2})	10
Pulse width τ_P fs	$\tau_P = 200$
The ambient water temperature T_∞(K)	300
The boiling temperature T_{boild} (K)	373

Important remark: The initial fluence value of $F_P = 5$ J/m^2 give rise to nanobubble nucleation; consequently, this value was increased to $F_P = 10$ J/m^2 in the following simulation.

To solve the Rayleigh–Plesset equation, we used three approaches:

- The first approach is based on the simplified Rayleigh–Plesset equation presented in Eq. (2.24) of Chapter 2, where $\mu_L = S = 0$ and the internal bubble pressure is assumed to be constant.
- The second approach is based on the complete Rayleigh–Plesset equation presented in Eq. (2.21) of Chapter 2, where $\mu_L \neq S \neq 0$ and the internal bubble pressure that we obtained using Clausius-Clapeyron model presented in Eq. (2.26) of Chapter 2 for the maximum temperature reached at the gold–water interface.
- The third approach is based on the complete Rayleigh–Plesset equation presented in Eq. (2.21) of Chapter 2, where $\mu_L \neq S \neq 0$ and the internal bubble pressure that we obtained using Clausius-Clapeyron model presented in Eq. (2.26) of Chapter 2 for the time-dependent variation of the temperature T at the nanoparticle–water interface.

Table 3.3: The parameters of Clausius-Clapeyron model for vapor pressure.

Physical parameters	**Value**
The reference vapor pressure P_{ref} (Pa)	10^5
The reference temperature T_{ref} (K)	373
The universal gas constant R_{gas} ($\mathrm{Jmol^{-1}\,K^{-1}}$)	8,314
The molar enthalpy of vaporization of water ΔH_v ($\mathrm{Jmol^{-1}}$)	$\Delta H_v = L_v \times M$
Latent heat of vaporization L_v ($\mathrm{Jkg^{-1}}$)	$2{,}26 \times 10^6$
Molar mass of water M ($\mathrm{kgmol^{-1}}$)	18×10^{-3}

We present the Python code that we developed and used to model the Rayleigh–Plesset equation for the three approaches. The corresponding plots are shown in Figures 3.4, 3.5, and 3.6.

In our code, we used the predefined solve_ivp function from the SciPy library, which is based on Runge–Kutta methods, to numerically solve the initial value problems associated with both the Two-Temperature Model (TTM) describing the temperature evolution inside the nanoparticle and the Rayleigh–Plesset equation governing cavitation around the nanoparticle. By default, solve_ivp employs the adaptive Runge–Kutta RK45 method for the numerical integration of ordinary differential equations.

The performed Python code consists of three interdependent modules, each addressing a specific problem: data, TTM solution, and Rayleigh–Plesset equation solution.

Code Python: Data Simulation (part 1)

```
import numpy as np
import matplotlib.pyplot as plt
from scipy.integrate import solve_ivp

# Physical Parameters
g=2.2e16                    # Electron-phonon coupling constant
tau=200e-15                 # Laser pulse duration
sigma_abs=10319.94e-18      # Maximum absorption cross-section
rho_gold=1.93e4             # Gold density
a=30e-9                     # Nanoparticle radius
Fpulse=10                   # Laser fluence
Tboild=373                  # Water boiling temperature
Lv =2.26e6                  # Latent heat of vaporization
M=18e-3                     # Molar mass of water
Rg=8.314                    # Ideal gas constant
DH_vap=Lv*M/Rg              # Enthalpy of vaporization
Eabs=sigma_abs*Fpulse       # Absorbed energy
kw=0.61                     # Thermal conductivity of water
Tf=300                      # Ambient water temperature
pi=np.pi
# Geometric parameters of the nanoparticle
Vp=(4/3) * pi * a**3        # Volume of the nanoparticle
Sp=4*pi*a**2                # Surface area of the nanoparticle
GG=105e6                    # thermal conductance
# Time
t0=0
t1=1000e-12
dt=tau/20
time=np.arange(t0, t1,dt)
n=len(time)
tdebut=t0
tfin=t1
```

Code Python: Two temperatures model (part 2)

```
# TTM model
def TTM(t, Y):
    Te, Tl = Y
    # Laser intensity profile (Gaussian)
    I0 = np.exp(-4 * np.log(2) * (t - 2 * tau)**2 / tau**2)
    S = Eabs * I0 / (tau * Vp)
    # Electron heat capacity
    Ce = 70 * Te
    # Lattice heat capacity
    CL = (109.579 + 0.128 * Tl - 3.4e-4 * Tl**2 + 5.24e-7 * Tl**3 - 3.93e-10 * Tl**4 + 1.17e-13 *
Tl**5)
    CL = rho_gold * CL
    # Heat transfered to water
    Q = 2 * pi * a * kw * Tf * (((Tl / Tf)**2) - 1)
    # ODE equations for electron and lattice temperatures
    dTe = -g * (Te - Tl) / Ce + S / Ce
    dTl = (g * (Te - Tl)) / CL - (Q / Vp) / CL
    return [dTe, dTl]
# Initial conditions
Te0 = 300
Tl0 = 300
Ts0 = 300
y0 = [Te0, Tl0]
# Resolution of TTM
sol = solve_ivp(TTM, [tdebut,tfin], y0, t_eval=time, max_step=dt)
t = sol.t * 1e12
Q = 2 * pi * a * kw * Tf * ((sol.y[1] / Tf)**2 - 1)
Ts = sol.y[1] - Q / (GG * Sp)                    # interrface temperature
Te = sol.y[0]                                     # Electron temperature
Tl = sol.y[1]                                     # Lattice temperature

#  Affichage
plt.figure(figsize=(10, 6))
plt.plot(sol.t * 1e12, sol.y[0], label="Température des électrons (Te)")
plt.plot(sol.t * 1e12, sol.y[1], label="Température du réseau (Tl)")
plt.axhline(Tboild, color='r', linestyle='--', label='Seuil d'ébullition (eau)')
plt.xlabel("Temps (ps)")
plt.ylabel("Température (K)")
plt.title("Modèle à deux températures (TTM) - échauffement par impulsion laser")
plt.legend()
plt.grid(True)
plt.show()
plt.plot(t,Ts)  # evolution de  # interrface temperature
plt.show()
```

Code Python : Rayleigh Plesset Equation (part 3)

```
#  Détection seuil de nanobulle Rayleigh Plesset
bulle_active = np.any(Ts > Tboild)
print(bulle_active )
# Température d'interface au moment du pic (nucléation)

Tnuc = float(np.max(Ts))
print(Tnuc)

#  Si bulle formée, lancer Rayleigh–Plesset
if bulle_active:
   print(" Nanobulle formée, simulation de sa croissance...")
   # Paramètres liquide / bulle
   P0= 1e5                 # Ambient pressure
   rho = 1000              # Liquid density of water
   sigma = 0.072           # Surface tension of water
   mu = 1e-3               # Dynamic viscosity of water
   R0 = 30e-9              # Initial bubble radius
   Tref = 373              # Reference temperature
   Pref = 1e5              # Reference pressure
   Lv =2.26e6              # Latent heat of vaporization
   M=18e-3                 # Molar mass of water
   R_gaz=8.314             # Ideal gas constant
  DH_vap=Lv*M              # Enthalpy of vaporization
   V0 = 0                  # Initial bubble wall velocity

# Vapor pressure calculation using Clausius-Clapeyron equation
   Pb = Pref * np.exp(-(DH_vap) * (1.0/Tnuc - 1.0/Tref))
   # Équation de Rayleigh–Plesset complete
   def RP(t, y):
      R, V = y
      dR = V
      dV = (Pb - P0 - 2*sigma/R - 4*mu*V/R) / (rho * R) - 1.5 * V**2 / R
      return [dR, dV]

   t_bulle = np.linspace(0, 2e-9, 100)
   sol_bulle = solve_ivp(RP, (0, 2e-9), [R0, V0], t_eval=t_bulle, method="RK45", max_step=1e-10)
   Rt = sol_bulle.y[0] * 1e9    # Conversion en nm
   tb = sol_bulle.t * 1e9      # Temps en ns

   #  Affichage bulle
   plt.figure(figsize=(7, 5))
   plt.plot(tb, Rt)
   plt.xlabel("Temps (ns)")
   plt.ylabel("Rayon de la bulle (nm)")
   plt.title("Croissance de la nanobulle")
   plt.grid()
   plt.tight_layout()
   plt.show()

else:
   print(" Pas de nanobulle : T < 373K partout")
```

First, the cavitation is modelled by the simplified Rayleigh–Plesset equation (surface tension and viscosity of water neglected), for a constant vapor pressure P_b. Figure 3.4 shows the nanobubble radius as a function of time for several constant values of the bubble vapor pressure. The selected vapor pressure values were kept constant and chosen to be slightly higher than the ambient pressure.

In the Figure 3.4: the evolution of the nanobubble radius as function of time (ns) using Simplified Rayleigh-Plesset model for several constant values of the bubble vapor pressure.

- All nanobubbles start with the same initial radius 30nm and subsequently expand over time.
- The figure illustrates the effect of vapor pressure on nanobubble dynamics. It can be observed that as the imposed vapor pressure inside the bubble increases, the expansion of the bubble radius becomes faster and more pronounced over time.
  - ✓ For $P_b = 1.2 \times 10^5$ Pa: the bubble radius reaches approximately 33,5 nm.
  - ✓ For $P_b = 1.5 \times 10^5$ Pa: the radius increases to about 33 nm.
  - ✓ For $P_b = 1.7 \times 10^5$ Pa: the bubble radius attains approximately 34,5 nm.

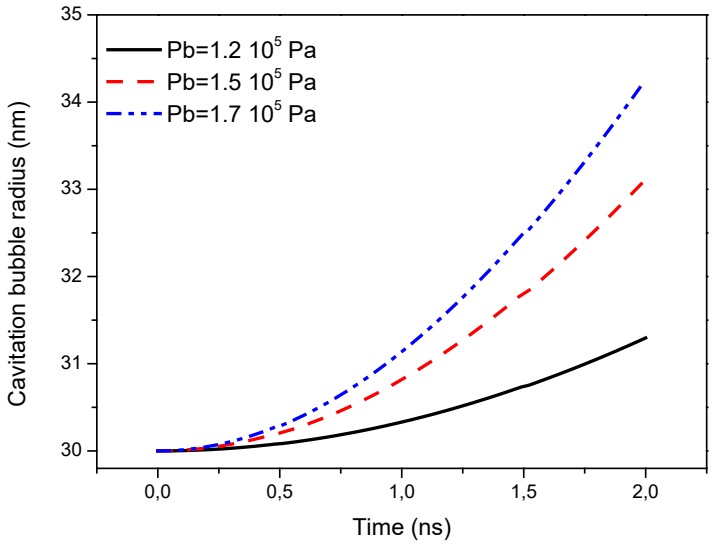

Figure 3.4: Evolution of the nanobubble radius as a function of time using Simplified Rayleigh-Plesset model for several constant values of the bubble vapor pressure.

Conclusion: Neglecting the effects of viscosity and surface tension leads to the absence of resistance to bubble growth, making its dynamics subject only to pressure force.

In the following, we consider, the cavitation modelled by the complete Rayleigh–Plesset equation, accounting for the surface tension and viscosity of the aqueous medium, for a vapor pressure Pb as a function of the vapor temperature T.

The Clausius–Clapeyron model (CC model) is chosen to describe the vapor pressure as a function of T within the nanobubble. In this case, the maximum temperature reached at the gold–water interface can be adopted as the reference value. This maximum temperature is taken as constant.

For comparison, both cavitation regimes are reported in Fig.3.5: the first is modelled with a constant pressure $P_b = 2 \times 10^5\, Pa$, neglecting the fluid parameters, while the second is modelled with a vapor pressure that depends on the vapor temperature.

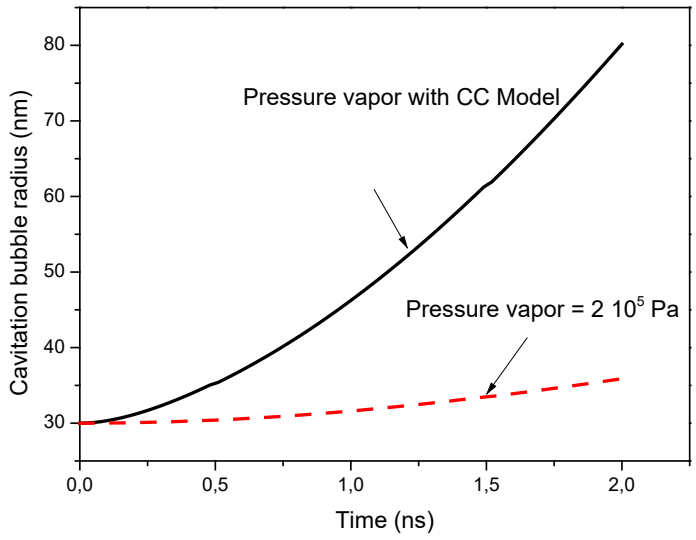

Figure 3.5: Evolution of the nanobubble radius as a function of time using Simplified Rayleigh-Plesset model for $P_b = 2 \times 10^5$ Pa and Complete Rayleigh-Plesset model using Clausius–Clapeyron model (CC) as function of the maximum temperature reached at the gold–water interface Ts.

In the Figure 3.5: the evolution of the nanobubble radius as function of time (ns) using Simplified Rayleigh-Plesset model for $P_b = 1.2 \times 10^5$ Pa and Complete Rayleigh-Plesset model using Clausius–Clapeyron model as function of the maximum temperature reached at the gold–water interface Ts.

- For the constant-pressure case $P_b = 2 \times 10^5$ Pa: the nanobubble exhibits weak expansion, reaching approximately 35 nm because the presence of viscosity and surface tension effects resists nanobubble growth.
- For the Clausius–Clapeyron (CC) model the bubble dynamics change significantly. The growth becomes strongly enhanced and nearly exponential, leading to a rapid increase in the radius up to approximately 80 nm in 2 ns.

In last part of simulation, the complete set of temperature values T, provided in tabular form, is used to construct a polynomial function through Lagrange interpolation. This interpolated expression is then substituted for the initially constant value used in Fig.3.5. Figure 3.6 thus represents the cavitation and collapse of the nanobubble.

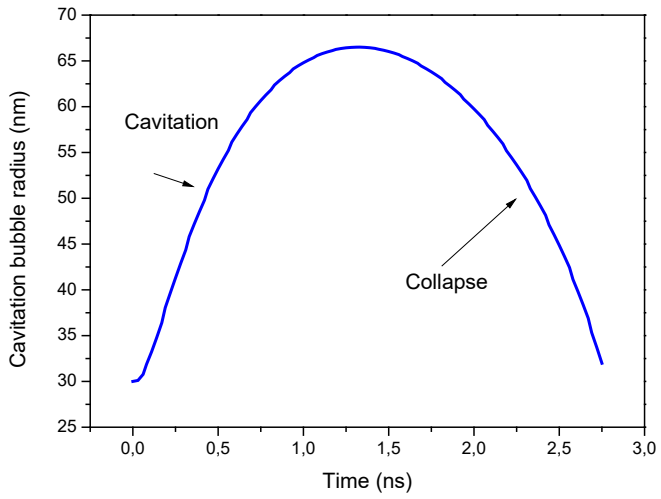

Figure 3.6: Evolution of the nanobubble radius as a function of time using Complete Rayleigh-Plesset model with Clausius–Clapeyron model as function of varying temperatures of interface Ts at the gold–water interface depending on time.

In the Figure 3.6: Evolution of the nanobubble radius as a function of time using Complete Rayleigh-Plesset model with Clausius–Clapeyron model as function of varying temperatures of interface Ts at the gold–water interface depending on time.

- At the beginning of the process, the bubble radius increases rapidly from approximately 30 nm, indicating the onset of cavitation and bubble growth due to vapor generation at the gold–water interface.

- As the interfacial temperature rises, the vapor pressure inside the bubble increases, promoting its expansion. The radius reaches a maximum value of about 65 nm at around 1.4 ns, corresponding to the maximum expansion stage.
- After this point, the bubble begins to collapse where the radius gradually decreases until it returns to nearly its initial value at approximately 2.8 ns.

The simulation code demonstrated that the laser parameters, particularly the laser fluence, are directly related to the occurrence of cavitation. By keeping all geometric parameters and the pulse duration constant, the influence of fluence on the thermal response of the medium can be clearly observed. The results indicate that for fluence values $Fp < 10/m^2$, the nucleation threshold temperature of 552 K is not reached. Consequently, vapor bubble nucleation does not occur, and no cavitation is generated under these conditions. These findings confirm that laser fluence, along with other parameters such as particle size and absorption cross-section, plays a key role in governing the generation of cavitation phenomena.

3.6 Conclusion:

In this chapter, a numerical study of laser-induced nanobubble generation around a gold nanoparticle was presented. The optical absorption properties of the nanoparticle were first analyzed, followed by the investigation of its thermal response using the Two-Temperature Model (TTM). The results showed that laser irradiation leads to a significant increase in temperature, which is transferred to the surrounding water and can exceed the boiling point at the Au/water interface. Under these conditions, vapor nanobubbles are generated and their dynamics were studied using the Rayleigh–Plesset equation. The simulations demonstrated that the bubble growth strongly depends on the vapor pressure using by Clausius–Clapeyron model and the thermal conditions at the interface. Overall, the obtained results provide a better understanding of the physical mechanisms involved in laser-induced nanocavitation around plasmonic nanoparticles.

References of Chapter 3

[1] A. N. Volkov, C. Sevilla, and L. V. Zhigilei, "Numerical modeling of short pulse laser interaction with Au nanoparticle surrounded by water," *Appl. Surf. Sci.*, 2007, doi: 10.1016/j.apsusc.2007.01.112

[2] R. Gan, H. Fan, Z. Wei, H. Liu, and A. Et., "Photothermal Response of Hollow Gold Nanorods under Femtosecond Laser Irradiation," *Nanomaterials*, 2019, doi: 10.3390/nano9050711

[3] O. Ekici, R. K. Harrison, N. J. Durr, D. S. Eversole, and A. Et., "Thermal analysis of gold nanorods heated with femtosecond laser pulses," *J. Phys. Appl. Phys.*, 2008, doi: 10.1088/0022-3727/41/18/185501

[4] R. R. Letfullin, C. B. Iversen, and T. F. George, "Modeling nanophotothermal therapy: kinetics of thermal ablation of healthy and cancerous cell organelles and gold nanoparticles," *Nanomedicine Nanotechnol.*, 2011, doi: 10.1016/j.nano.2010.06.011

[5] E. Majchrzak and J. Dziatkiewicz, "Analysis of ultrashort laser pulse interactions with metal films using a two-temperature model," Journal of Applied Mathematics and Computational Mechanics, vol. 14, no. 2, pp. 31–39, 2015, doi: 10.17512/jamcm.2015.2.04

General Conclusion

This work presents a numerical study of laser-induced nanocavitation around gold nanoparticles immersed in water. Using femtosecond laser pulses, the nanoparticle absorbs light energy through its localized surface plasmon resonance, leading to ultrafast heating of the electron and lattice subsystems. This thermal response is described by the Two-Temperature Model, which governs the energy exchange between electrons and the gold lattice, and determines the temperature evolution at the nanoparticle–water interface.

When the interface temperature exceeds a critical threshold — associated with explosive boiling or spinodal decomposition of the surrounding liquid — a vapor nanobubble nucleates around the nanoparticle. The growth and collapse dynamics of this bubble are governed by the Rayleigh–Plesset equation, which accounts for the vapor pressure inside the bubble, the ambient liquid pressure, surface tension, and viscosity. The vapor pressure is evaluated dynamically through the Clausius–Clapeyron relation, directly coupling the bubble dynamics to the thermal state of the interface.

The full simulation chain was implemented in Python, combining the optical cross-section calculation via the Drude–Lorentz model and the quasi-static approximation, the numerical integration of the Two-Temperature Model, and the resolution of the Rayleigh–Plesset equation. The results illustrate how laser parameters and thermodynamic conditions of the surrounding medium jointly control the nucleation threshold, the maximum bubble radius, and the collapse time of the vapor nanobubble.

Overall, this work provides a comprehensive understanding of the optical absorption, ultrafast heating, cavitation mechanisms, and nanobubble dynamics induced by femtosecond laser irradiation of gold nanoparticles. These findings constitute a useful basis for future investigations

Future work could incorporate more realistic geometries, such as core-shell nanostructures ($Au@SiO_2$) and examine how the shell thickness and material properties influence the nucleation threshold and bubble dynamics. The coupling between the Rayleigh–Plesset equation and a full heat diffusion model in the liquid — rather than relying solely on the interface temperature, would also provide a more rigorous description of the thermal boundary layer driving bubble growth.

Abstract

This work investigates the interaction between femtosecond laser pulses and gold nanoparticles immersed in water. The optical properties of gold nanoparticles were studied using the Drude, modified Drude, and Drude–Lorentz models, while the quasi-static approximation was employed to calculate their optical cross-sections and localized surface plasmon resonance (LSPR). The thermal response of the nanoparticles was analyzed using the Two-Temperature Model (TTM), allowing the determination of electron, lattice, and gold–water interface temperatures. The conditions leading to explosive boiling, cavitation, and nanobubble nucleation were then examined. Finally, the Rayleigh–Plesset equation was used to model the growth and collapse dynamics of laser-induced vapor nanobubbles. The results provide a comprehensive understanding of the optical, thermal, and hydrodynamic processes involved and highlight the potential of gold nanoparticles for photothermal and biomedical applications.

Keywords: Cavitation, Nanobubbles, Rayleigh–Plesset Equation, Gold Nanoparticles, Femtosecond laser, Drude–Lorentz Model, Quasi-static Approximation, TTM.

Résumé

Ce travail porte sur l'étude de l'interaction entre des impulsions laser femtosecondes et des nanoparticules d'or immergées dans l'eau. Les propriétés optiques des nanoparticules ont été étudiées à l'aide des modèles de Drude, Drude modifié et Drude–Lorentz, tandis que l'approximation quasi-statique a permis de calculer les sections efficaces optiques et la résonance plasmonique de surface localisée (LSPR). La réponse thermique a été analysée à travers le modèle à deux températures (TTM), permettant de déterminer les températures électronique, du réseau cristallin et de l'interface or/eau. Les mécanismes conduisant à l'ébullition explosive, à la cavitation et à la nucléation des nanobulles ont ensuite été examinés. Enfin, l'équation de Rayleigh–Plesset a été utilisée pour modéliser la croissance et l'effondrement des nanobulles de vapeur induites par laser. Les résultats obtenus permettent une meilleure compréhension des phénomènes optiques, thermiques et hydrodynamiques mis en jeu et ouvrent des perspectives dans les applications photothermiques et biomédicales.

Mots-clés : Cavitation, Nanobulles, Equation de Rayleigh–Plesset, Nanoparticules d'or, Laser Femtoseconde, Modèle de Drude–Lorentz, Approximation quasi-statique, TTM.

الملخص

تتناول هذه الدراسة تفاعل نبضات الليزر الفيمتوثانية مع الجسيمات النانوية الذهبية المغمورة في الماء. تمت دراسة الخصائص البصرية لهذه الجسيمات باستخدام نماذج درود، درود المعدل، ودرود–لورنتز، كما استُخدم التقريب شبه الساكن لحساب المقاطع البصرية وظاهرة الرنين البلازموني السطحي الموضعي .(LSPR) وتم تحليل الاستجابة الحرارية للجسيمات النانوية بواسطة نموذج درجتي الحرارة (TTM) لتحديد درجات حرارة الإلكترونات والشبكة البلورية وواجهة الذهب/الماء. بعد ذلك، تمت دراسة الشروط المؤدية إلى الغليان الانفجاري والتجويف وتكوّن الفقاعات النانوية البخارية. وأخيرًا، استُخدمت معادلة رايلي–بليسيت لوصف ديناميكية نمو وانهيار هذه الفقاعات. وقد ساهمت النتائج في تقديم فهم متكامل للظواهر البصرية والحرارية والهيدروديناميكية المرتبطة بتسخين الجسيمات النانوية الذهبية بالليزر، مع إبراز أهميتها في التطبيقات الطبية والعلاج الضوئي الحراري.

الكلمات المفتاحية :الجسيمات النانوية الذهبية، الليزر الفيمتوثاني، نموذج درود–لورنتز، التقريب شبه الساكن، نموذج درجتي الحرارة، التجويف، الفقاعات النانوية، معادلة رايلي–بليسيت.